Modelling the breakup of solid aggregates in turbulent flows

MATTHÄUS U. BÄBLER[1], MASSIMO MORBIDELLI[1] AND JERZY BAŁDYGA[2]

[1]Institute for Chemical and Bioengineering, ETH Zurich, 8093 Zurich, Switzerland
massimo.morbidelli@chem.ethz.ch

[2]Faculty of Chemical and Process Engineering, Warsaw University of Technology,
Waryǹskiego 1, PL 00-645 Warsaw, Poland

The breakup of solid aggregates suspended in a turbulent flow is considered. The aggregates are assumed to be small with respect to the Kolmogorov length scale and the flow is assumed to be homogeneous. Further, it is assumed that breakup is caused by hydrodynamic stresses acting on the aggregates, and breakup is therefore assumed to follow a first-order kinetic where $K_B(x)$ is the breakup rate function and x is the aggregate mass. To model $K_B(x)$, it is assumed that an aggregate breaks instantaneously when the surrounding flow is violent enough to create a hydrodynamic stress that exceeds a critical value required to break the aggregate. For aggregates smaller than the Kolmogorov length scale the hydrodynamic stress is determined by the viscosity and local energy dissipation rate whose fluctuations are highly intermittent. Hence, the first-order breakup kinetics are governed by the frequency with which the local energy dissipation rate exceeds a critical value (that corresponds to the critical stress). A multifractal model is adopted to describe the statistical properties of the local energy dissipation rate, and a power-law relation is used to relate the critical energy dissipation rate above which breakup occurs to the aggregate mass. The model leads to an expression for $K_B(x)$ that is zero below a limiting aggregate mass, and diverges for $x \rightarrow \infty$. When simulating the breakup process, the former leads to an asymptotic mean aggregate size whose scaling with the mean energy dissipation rate differs by one third from the scaling expected in a non-fluctuating flow.

1. Introduction

Breakup of small suspended aggregates (clusters, flocs) due to hydrodynamic stresses induced by fluid flow is crucial to both aggregation (coagulation, flocculation) and dispersion processes. The former finds broad application in solid–liquid separation where the transformation of particles in the colloidal size range into aggregates of a few micrometres to millimetres in size improves the performance of any separator. Aggregation is usually performed in an agitated device where vigorous stirring leads to aggregate breakup which limits the formation of large aggregates. Regarding the reverse process, i.e. dispersing a solid into a liquid, aggregate breakup by vigorous stirring becomes the controlling mechanism.

This paper addresses the modelling of breakup kinetics of solid aggregates in a homogeneous turbulent flow. It is generally assumed that breakup is a first-order kinetic process, and, accordingly, the population balance equation describing the

evolution of the cluster mass distribution (CMD) can be written

$$\frac{\partial c(x,t)}{\partial t} = -K_B(x)c(x,t) + \int_x^\infty g(x,y)K_B(y,t)c(y,t)\,\mathrm{d}y, \qquad (1.1)$$

where $c(x,t)$ is the CMD, x is the cluster mass normalized by the mass of the primary particle that forms the aggregate, t is the time, $K_B(x)$ is the breakup rate function, and $g(x,y)$ is the fragment mass distribution (FMD). Hence, the number of fragments of mass $(x,x+\mathrm{d}x)$ formed by the breakup of a cluster mass y is $g(x,y)\mathrm{d}x$. Although the process described by (1.1) is relevant to both aggregation and dispersion, modelling strategies to describe $K_B(x)$ and $g(x,y)$ are scarce in the literature. Based on ideas of Delichatsios (Delichatsios 1975; Delichatsios & Probstein 1976), Kusters (1991) and Flesch, Spicer & Pratsinis (1999) developed an exponential breakup rate function,

$$K_B(x) = \sqrt{\frac{4}{15\pi}} \left(\frac{\langle \varepsilon \rangle}{\nu} \right)^{1/2} \exp\left(-\frac{B[a(x)]^{-1/p}}{\langle \varepsilon \rangle} \right), \qquad (1.2)$$

where $\langle \varepsilon \rangle$ is the mean energy dissipation rate, ν is the kinematic viscosity, $a(x)$ is the characteristic size of an aggregate of mass x, and B and p are parameters that describe the response of an aggregate to an applied hydrodynamic stress. Equation (1.2) applies to aggregates smaller than the Kolmogorov length scale, $\eta = (\nu^3/\langle \varepsilon \rangle)^{1/4}$, and it assumes that the force that drives breakup (i.e. the mechanism that creates stresses acting on the aggregate) fluctuates with a Gaussian distribution. In a simpler framework, it is assumed that breakup is faster the more vigorous the stirring and that large aggregates are more likely to break than small ones, which is translated into a power law (Pandya & Spielman 1982; Spicer & Pratsinis 1996),

$$K_B(x) = K_0 G^D [a(x)]^E, \qquad (1.3)$$

where K_0 is a constant, G is the characteristic velocity gradient of the flow (shear rate), and D and E are positive empirical parameters that depend on the particular system under investigation.

Recently, shortcomings of the rate functions given by (1.2) and (1.3) have been found. Regarding the power-law breakup rate function given by (1.3), Bäbler & Morbidelli (2007) showed that the moments of the steady-state CMD that results from a balance between aggregation and breakup, where the latter is described by (1.3), exhibit power-law scaling with both G and the solid volume fraction ϕ; the scaling exponents depend on D and E. Analysis of experimental data revealed that the scaling of the steady-state moments of the CMD is different for G and ϕ than predicted by the model, from which it is concluded that (1.3) is not flexible enough to describe the experimental findings. Further, the lack of any physical picture behind (1.3) is unsatisfactory because its parameters cannot be estimated other than by solving (1.1) and fitting D and E to experimental data. Regarding the exponential breakup rate function given by (1.2), for $a(x) \gg (B/\langle \varepsilon \rangle)^p$ we have that $K_B(x)$ converges to a constant, which is unsatisfactory. Breakup that is governed by a constant breakup rate function cannot compete with aggregation (Bäbler & Morbidelli 2007), whose rate function is strongly dependent on the size of the colliding aggregates (Saffman & Turner 1956), and no steady-state CMD would result from a balance of aggregation and breakup once the aggregates grow larger than $(B/\langle \varepsilon \rangle)^p$. (There is still the possibility that the steady state observed in the aggregation of a suspension of primary particles in a turbulent flow results from an aggregation efficiency that drops to zero at a certain aggregate size (Brakalov 1987) but this is not in agreement with experimental findings (Moussa *et al.* 2007) and theoretical considerations (Bäbler

et al. 2006; Bäbler 2008)). Finally, experiments (Moussa *et al.* 2007; Sonntag & Russel 1986; Kobayashi, Adachi & Ooi 1999) and theoretical studies (Adler & Mills 1979; Sonntag & Russel 1987*b*; Horwatt, Feke & Manas-Zloczower 1992*a*; Higashitani, Iimura & Sanda 2001) suggest the existence of a critical aggregate size below which aggregates in a given flow do not break, which is not rigorously included in (1.2) and (1.3) (for which $K_B(x) > 0$ for $x > 0$).

In this paper, a modelling strategy is proposed that allows us to derive expressions for $K_B(x)$ and $g(x, y)$ in a physically sound framework (§ 2). It is assumed that the first-order breakup kinetics are governed by the turbulent fluctuations where only turbulent events that are violent enough lead to breakup. The magnitude of a turbulent event required to cause breakup is thereby determined by the properties of the aggregate and depends in particular on the aggregate mass. To describe the turbulent fluctuations a multifractal model is adopted which provides a sufficient description of the fine-scale turbulence (§ 3). In particular, the multifractal model accounts for the fine-scale intermittency that causes a Reynolds number dependence of the statistical properties of the flow. Further, a power-law relation is used to relate the critical magnitude of a turbulent event that causes breakup to the mass of an aggregate (§ 4). The resulting breakup rate function presented in § 5 is substantially different to (1.2) and (1.3) in that $K_B(x) = 0$ and $K_B(x) \rightarrow \infty$ below and above a certain limiting aggregate size, respectively. Further, $K_B(x)$ exhibits a Reynolds number dependence due to intermittency that is missing in the present models. Finally, it will be shown that when turbulence is modelled using a Gaussian velocity gradient, the modelling framework presented leads to an expression for $K_B(x)$ that in the limits of $x \rightarrow 0$ and $x \rightarrow \infty$ reduces to an exponential function and a power law that are formally identical to (1.2) and (1.3), respectively.

2. Model development

2.1. *Breakup rate function*

Let us consider an ensemble of aggregates suspended in an incompressible turbulent flow. The flow is assumed to be statistically stationary and homogeneous in spatial coordinates, and it is assumed that the suspension is sufficiently diluted that the statistical properties of the flow are not altered by the presence of the aggregates. It is assumed that the aggregate Reynolds number $R_p = Ga^2/\nu \ll 1$ and the aggregate Stokes number $St_p = \tau_p G \ll 1$, where τ_p is the relaxation time of the aggregate motion, i.e. the time it takes the aggregate to adjust its velocity to the velocity of the surrounding fluid flow, which is computed as (Hinze 1975)

$$\tau_p = \frac{(2\rho_p/\rho_f + 1)a^2}{9\nu}, \tag{2.1}$$

where ρ_p and ρ_f are the density of the aggregate and the fluid phase, respectively. $St_p \ll 1$ implies that the aggregates have negligible inertia and that they adjust their velocity instantaneously to the surrounding flow. Thus, hydrodynamic stresses created by the drag due to acceleration of the aggregates are negligible. Also, this implies that the aggregate concentration field can be treated as statistically homogeneous. Further, $R_p \ll 1$ and $St_p \ll 1$ identifies the dominant mechanism for aggregate breakup to be due to viscous stresses caused by the local velocity gradient of the fluid flow. Breakup due to interparticle collisions appears unlikely in the present framework. An encounter between two aggregates assuming $R_p \ll 1$ and $St_p \ll 1$ is controlled by the viscous fluid motions in the vicinity of the aggregates. These cause a strong retardation and

a strong deflection of the relative aggregate trajectories (Batchelor & Green 1972; Bäbler *et al.* 2006; Joseph *et al.* 2001). The change resulting from a collision that creates enough momentum to break one of the aggregates is therefore negligible (this is not the case for heavy particles with finite inertia). Finally, estimating $G \approx (\langle \varepsilon \rangle / \nu)^{1/2}$, for a small density ratio the aforementioned conditions are equivalent to $a \ll \eta$, where $\eta = (\nu / \langle \epsilon \rangle)^{1/4}$ is the Kolmogorov length scale. Hence, the present model is applicable to small aggregates suspended in a liquid flow (e.g. for a suspension of polymeric aggregates in an aqueous turbulent flow with $\langle \varepsilon \rangle = 1$ m^2 s^{-3}, which is a typical value for industrial coagulators, we have $\rho_p / \rho_f \approx 0.9$–$2.2$ and $\eta \approx 30$ μm).

For aggregates smaller than the Kolmogorov length scale, the properties of the flow on the length scale of the aggregate are determined by the local energy dissipation rate and the viscosity. Thereby, the local energy dissipation rate is a fluctuating quantity whose fluctuations are highly intermittent (Batchelor & Townsend 1949; Meneveau & Sreenivasan 1991; Frisch 1995). That is, although the flow is statistically stationary and homogeneous and therefore the mean energy dissipation rate is distributed uniformly, in certain regions of space and time the local energy dissipation rate assumes values that are very different from the mean (for a proper definition of intermittency see Frisch 1995). These intense events appear irregularly as short-lived bursts, and their magnitude and frequency increases with increasing Reynolds number.

Let us continue by focusing on the breakup event. The time scale τ_ε denotes the duration over which the flow in the vicinity of an aggregate persists in a Lagrangian framework. The local flow is determined by the local velocity gradient, $\gamma \sim (\varepsilon / \nu)^{1/2}$, which is approximately constant on the length scale of the aggregate. Adopting a simplistic view, τ_ε is understood as the characteristic time of the smallest eddies of the flow (i.e. eddies of the size of the Kolmogorov length scale). Regarding the breakup event, it is assumed that its characteristic time is much shorter than τ_ε as originally suggested by Sonntag & Russel (1986, 1987c). In other words, it is assumed that the breakup event is instantaneous with respect to the characteristic time of the smallest eddies (the applicability of this assumption is discussed in the context of the aggregate response function in §4). The importance of this assumption in the modelling of droplet and bubble breakup was also pointed out by Risso (2000). The basic principle of the present model is then that breakup is caused only by eddies that are violent enough, i.e. pieces of fluid that exhibit a large velocity gradient. Accordingly, the breakup kinetics are governed by the frequency of appearance of these violent eddies, that is, the turbulent fluctuations of the local velocity gradient. To understand this, let us consider an aggregate suspension where all aggregates are assumed to be identical. If there were no fluctuations in the local velocity gradient (and hence, no fluctuations in the stress exerted on the aggregates) we have the situation that all aggregates would be in the same environment. Hence, they would either break within the characteristic time of the breakup event (which in the present case is identical for all aggregates) or survive, depending on the magnitude of the applied stress. On the other hand, if we allow for fluctuations in the velocity gradient the (macroscopic) rate of breakup is determined by the frequency with which the stress exceeds a certain critical value above which the aggregates break. It is this latter principle that is developed within this paper.

Let us interpret the intermittent character of the energy dissipation rate field in such a way that there are intense regions embedded in a field of low intensity. The intense regions are thereby characterized by their capability to break the aggregates. To be precise, in the intense regions $\varepsilon > \varepsilon_{cr}$, where ε_{cr} is a critical energy dissipation rate (that corresponds to a critical velocity gradient and, accordingly, to a critical
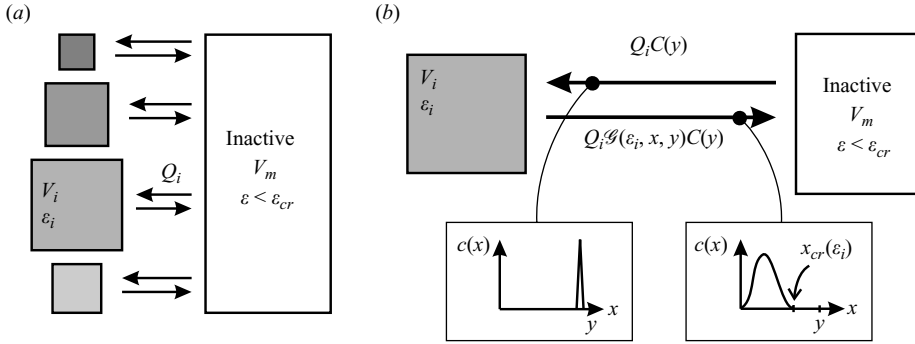
(a)

(b)

FIGURE 1. (*a*) Intermittency creates regions of high energy dissipation rate (represented by the shaded boxes) where the aggregates are broken up. (*b*) The fragments resulting from the breakup of an aggregate of mass y in region i have a mass distribution $\mathcal{G}(\varepsilon_i, x, y)$.

stress) above which the aggregates break. $\varepsilon_{cr} = \varepsilon_{cr}(x)$ is assumed to depend solely on the properties of the aggregates. The region of fluid with $\varepsilon \leqslant \varepsilon_{cr}(x)$, where the aggregates do not break, is denoted as inactive. It is assumed that the intense regions continuously engulf fluid from the inactive environment at a rate Q_i, where the index i refers to the region characterized by a local energy dissipation rate ε_i. The detailed mechanism of engulfment and the evolution of the region of active fluid is of minor importance for the present analysis (analogous expressions are derived if it is assumed that an intense region forms from an arbitrary parcel of fluid of volume V_i that remains segregated from the bulk flow for a time $\tau_{\varepsilon,i}$). Figure 1(*a*) illustrates this scenario, where the intense regions are shown by the shaded boxes. A simple material balance of aggregates of mass x in the inactive fluid is

$$V_m \frac{\mathrm{d}C_m}{\mathrm{d}t} = -\sum_i Q_i C_m, \qquad (2.2)$$

where C_m and V_m denote the aggregate concentration and the volume of the inactive fluid, respectively. The aggregates break instantaneously when entering an intense region. As a consequence of this, the material balance of an intense region is $V_i \mathrm{d}C_i/\mathrm{d}t = 0$, where C_i and V_i are the concentration and the volume of region i, respectively. The latter material balance has the trivial solution $C_i = 0$, i.e. aggregates of mass x cannot exist in the intense region. The rate of decay of the total number of aggregates, N, is then governed by

$$\frac{\mathrm{d}N}{\mathrm{d}t} = V_m \frac{\mathrm{d}C_m}{\mathrm{d}t} + \sum_i V_i \frac{\mathrm{d}C_i}{\mathrm{d}t}, \qquad (2.3)$$

which equates to $N = N_0 \exp(-K_B t)$, where N_0 is the initial number of particles in the inactive fluid and K_B is the breakup rate function

$$K_B = \sum_i Q_i / V_m. \qquad (2.4)$$

In what follows, Q_i and V_m are expressed through the properties of the flow. Q_i is the volume flow rate with which an intense region characterized by ε_i engulfs fluid from the environment. This is, expressed as
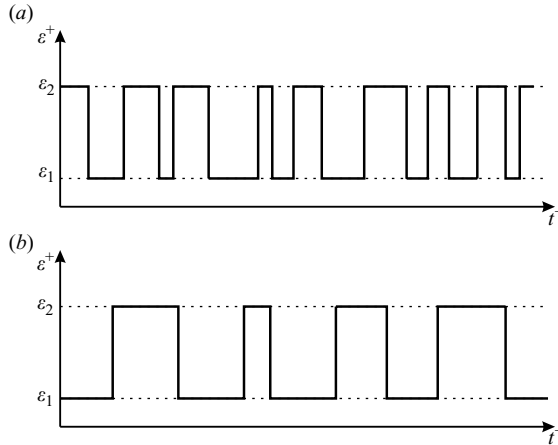
$$Q_i = V_i / \tau_{\varepsilon,i}, \qquad (2.5)$$

FIGURE 2. Energy dissipation rate along the particle trajectory in a degenerated field of energy dissipation rate. Variables superscripted by + indicate the Lagrangian frame.

where V_i is the volume of region i, i.e. the fraction of fluid with ε_i, is given by $V_i/V = p_\varepsilon(\varepsilon_i)\mathrm{d}\varepsilon$. Here, V is the total volume and $p_\varepsilon(\varepsilon)$ is the probability density function (PDF) of the local energy dissipation rate. The time scale τ_ε was introduced above as the time scale over which the flow on the length scale of the aggregate persists in a Lagrangian framework. To get an understanding of (2.5), let us consider a degenerated flow field where the local energy dissipation rate assumes either a value ε_1 or ε_2 and where there are particles moving in this field. Two very different realizations of the energy dissipation rate along a particle trajectory are sketched in figure 2. In case (*a*), the particle moves fast and it often switches from ε_1 to ε_2. In case (*b*), the particle moves slowly and it switches only occasionally between ε_1 and ε_2. When there are no preferential particles concentrations (which holds for particles with $St_p \ll 1$) the fraction of time the particle samples an energy dissipation rate between ε and $\varepsilon + \mathrm{d}\varepsilon$ is given by the PDF of ε (Tennekes & Lumley 1972; Borgas 1993) which is considered the same for the two cases. From this scenario, it is reasonable to assume that the volume flux of fluid from region ε_1 to region ε_2 is proportional to the average frequency with which the particles switch from ε_1 and ε_2, and further, that the average frequency with which the particles switch from ε_1 and ε_2 is inversely proportional to $\tau_\varepsilon(\varepsilon_2)$, i.e. the average time the particle spends in region ε_2 per passage. Hence, the volume flux is given by the volume of region ε_2 divided by $\tau_\varepsilon(\varepsilon_2)$. Finally, the volume of the inactive fluid, V_m, is the fraction of fluid with $\varepsilon \leqslant \varepsilon_{cr}(x)$ which is given by

$$V_m/V = \int_0^{\varepsilon_{cr}(x)} p_\varepsilon(\varepsilon)\,\mathrm{d}\varepsilon. \tag{2.6}$$

Combining these relations and expressing the sum in (2.4) through an integral, we finally obtain the breakup rate function:

$$K_B(x) = \frac{\displaystyle\int_{\varepsilon_{cr}(x)}^{\infty} p_\varepsilon(\varepsilon)/\tau_\varepsilon(\varepsilon)\,\mathrm{d}\varepsilon}{\displaystyle\int_0^{\varepsilon_{cr}(x)} p_\varepsilon(\varepsilon)\,\mathrm{d}\varepsilon}. \tag{2.7}$$

It is seen that the breakup rate function given by (2.7) contains three functions. These are on one hand the two functions representing turbulence, i.e. $p_\varepsilon(\varepsilon)$ and $\tau_\varepsilon(\varepsilon)$, which are only dependent on the properties of the flow. On the other hand, we have the aggregate response function $\varepsilon_{cr}(x)$ which is assumed to be only dependent on the properties of the aggregates. The elegance of the present model is thus the decomposition of the breakup problem into a turbulent part and a part addressing the aggregate mechanics, i.e. the response of an aggregate to an applied stress. Both these parts can be treated independently. It is noticed that this decomposition shows (2.7) to be substantially different to the so-called *eddy collision models* that are developed to describe the breakup of large fluid particles (i.e. bubbles and droplets with sizes in the inertial subrange of turbulence) (Prince & Blanch 1990; Tsouris & Tavlarides 1994; Luo & Svendson 1996). In these models the breakup rate function is given as the product of the collision frequency of a particle with eddies of comparable size and a breakup efficiency relating the energy required to break a droplet to the energy provided by the collision with the eddy. The resulting expression for K_B consists of an integral over all eddy sizes whose collisions lead to breakup. As pointed out by Lasheras *et al.* (2002) the range of eddies considered capable of breaking the particle (which essentially defines the integration boundaries) has a strong influence on the value of K_B and it is to a large extent arbitrary. Equation (2.7), on the other hand, does not rely on the notion of eddy collision and, additionally, the integration boundaries are well defined (the integration to infinity in the numerator of (2.7) is benign since $p_\varepsilon(\varepsilon)$ vanishes for $\varepsilon \to \infty$ as shown shortly).

Before addressing the two parts comprising (2.7), the present modelling framework is exploited to draw some conclusions about the FMD $g(x, y)$.

2.2. *Fragment mass distribution*

Let us return to the simple picture sketched in figure 1(*a*). Aggregates in the inactive fluid are engulfed into region i at a rate Q_i where they break. Let us assume the original aggregates have a mass y and the fragments leaving region i have a distribution $\mathscr{G}(\varepsilon_i, x, y)$, where $\mathscr{G}(\varepsilon_i, x, y)\mathrm{d}x$ is the number of fragments of mass $(x, x + \mathrm{d}x)$ resulting from the breakup of an aggregate of mass y in an intense region characterized by ε_i (figure 1*b*). Accordingly, $\mathscr{G}(\varepsilon_i, x, y)$ is referred to as the *elementary FMD*. To be consistent with our notion of instantaneous breakup, we have $\mathscr{G}(\varepsilon_i, x, y) = 0$ for $x > x_{cr}(\varepsilon_i)$ (and for $x > y$), where $x_{cr}(\varepsilon_i)$ is the inverse of the aggregate response function $\varepsilon_{cr}(x)$. Hence, the fragments that leave region i are all smaller than the maximum mass sustainable in region i. This assumes in particular that a series of breakup events leading to fragments smaller than $x_{cr}(\varepsilon_i)$ is also instantaneous. Accounting for all active regions, the global FMD, $g(x, y)$, to be used in (1.1) follows as

$$g(x, y) = \frac{\sum_i \mathscr{G}(\varepsilon_i, x, y)Q_i}{\sum_i Q_i}. \qquad (2.8)$$

Using $Q_i = V_i/\tau_\varepsilon(\varepsilon_i)$ and expressing V_i through the PDF of the local energy dissipation rate results in

$$g(x, y) = \frac{\displaystyle\int_{\varepsilon_{cr}(y)}^{\infty} \mathscr{G}(\varepsilon, x, y)p_\varepsilon(\varepsilon)/\tau_\varepsilon(\varepsilon)\,\mathrm{d}\varepsilon}{\displaystyle\int_{\varepsilon_{cr}(y)}^{\infty} p_\varepsilon(\varepsilon)/\tau_\varepsilon(\varepsilon)\,\mathrm{d}\varepsilon}, \quad x \leqslant y. \qquad (2.9)$$

Analogous to the breakup rate function (2.7), the FMD given by (2.9) decomposes the problem into a turbulent part represented by $p_\varepsilon(\varepsilon)$ and $\tau(\varepsilon)$ and a part depending

on the properties of the aggregates represented by $\mathscr{G}(\varepsilon, x, y)$. Unlike the aggregate response function $\varepsilon_{cr}(x)$, that is discussed shortly, the elementary FMD, $\mathscr{G}(\varepsilon, x, y)$, is difficult to model rigorously: $\mathscr{G}(\varepsilon, x, y)$ gives the statistics of the breakup of an individual (well-defined) aggregate of mass y in a (well-defined) flow of magnitude ε. Simulations or experiments designed to study the breakup of an individual aggregate must therefore be repeated several times in order to obtain a representative elementary FMD. Therefore, we propose two simple empirical forms of $\mathscr{G}(\varepsilon, x, y)$ which, for convenience, are presented within this section.

The first empirical model for $\mathscr{G}(\varepsilon, x, y)$ is a uniform FMD. That is, the probability that the breakup of an aggregate of mass $y > x_{cr}(\varepsilon)$ in a region characterized by ε leads to a fragment of mass $x \leqslant x_{cr}(\varepsilon)$ is uniform, i.e.

$$\mathscr{G}(\varepsilon, x, y) = \begin{cases} A_1, & x \leqslant x_{cr}(\varepsilon) \text{ and } y > x_{cr}(\varepsilon) \\ 0, & \text{otherwise} \end{cases} \quad (2.10)$$

where mass conservation, $\int_0^\infty x \, \mathscr{G}(\varepsilon, x, y) \, \mathrm{d}x = y$, imposes $A_1 = 2y/[x_{cr}(\varepsilon)]^2$. Substituting (2.10) into (2.9) leads to a global FMD:

$$g(x, y) = \left[\int_{\varepsilon_{cr}(y)}^{\varepsilon_{cr}(x)} \frac{p_\varepsilon(\varepsilon)}{\tau_\varepsilon(\varepsilon)} \frac{2y}{[x_{cr}(\varepsilon)]^2} \mathrm{d}\varepsilon \right] \left[\int_{\varepsilon_{cr}(y)}^\infty \frac{p_\varepsilon(\varepsilon)}{\tau_\varepsilon(\varepsilon)} \mathrm{d}\varepsilon \right]^{-1}, \quad x \leqslant y. \quad (2.11)$$

In the second empirical model for $\mathscr{G}(\varepsilon, x, y)$ it is assumed that the breakup of an aggregate of mass $y > x_{cr}(\varepsilon)$ in a region characterized by ε forms only fragments of mass $x_{cr}(\varepsilon)$. In the view of figure 1(b), the fragments leaving region i all assume the maximum mass that is allowed to survive in region i. This leads to an elementary FMD that is a Dirac delta function,

$$\mathscr{G}(\varepsilon, x, y) = A_2 \delta(x - x_{cr}(\varepsilon)), \quad y > x_{cr}(\varepsilon), \quad (2.12)$$

where mass conservation imposes $A_2 = y/x_{cr}(\varepsilon)$. Substituting (2.12) into (2.9) leads to a global FMD:

$$g(x, y) = \left[-\left(\frac{y}{x}\right) \frac{p_\varepsilon(\varepsilon_{cr}(x))}{\tau_\varepsilon(\varepsilon_{cr}(x))} \frac{\mathrm{d}\varepsilon_{cr}(x)}{\mathrm{d}x} \right] \left[\int_{\varepsilon_{cr}(y)}^\infty \frac{p_\varepsilon(\varepsilon)}{\tau_\varepsilon(\varepsilon)} \mathrm{d}\varepsilon \right]^{-1}, \quad x \leqslant y. \quad (2.13)$$

The two FMDs given by (2.11) and (2.13) contain the same three functions as (2.7) to represent turbulence and the aggregate mechanics. It will be shown later that the two FMDs differ substantially in the formation of small fragments but that they lead to similar predictions for large fragments. Moreover, their simple form allows an analytical treatment of the asymptotic CMD, $c(x, t)$ as $t \to \infty$, resulting from (1.1). Finally, we note that we did not use the number of fragments to characterize the two empirical models for the elementary FMDs, (2.10) and (2.12). This number is given by $w = \int_0^\infty \mathscr{G}(\varepsilon, x, y) \mathrm{d}x$ and it is seen that w depends on the mass of the breaking aggregate, i.e. y. The elementary FMDs (and the global FMDs) proposed in this work are therefore non-self similar (i.e. $\mathscr{G}(\varepsilon, x, y)$ cannot be expressed as a unique function of x/y). Self-similar FMDs are used frequently in the literature (Spicer & Pratsinis 1996; Flesch *et al.* 1999; Bäbler & Morbidelli 2007) but there is no physical constraint that imposes a self-similar FMD.

3. Turbulent part of $K_B(x)$

This section treats the turbulent part of the breakup model introduced in §2. That is, expressions for the PDF of the local energy dissipation rate, $p_\varepsilon(\varepsilon)$, and the time

scale $\tau_\varepsilon(\varepsilon)$ appearing in (2.7), (2.11) and (2.13) are provided. A multifractal model is adopted to describe $p_\varepsilon(\varepsilon)$, whereas for $\tau_\varepsilon(\varepsilon)$ we will refer to Lagrangian statistics.

3.1. *A multifractal model for $p_\varepsilon(\varepsilon)$*

3.1.1. *Multifractal formalism*

(Multi)fractal models provide a statistical description of fine-scale turbulence, that is, phenomena taking place in the equilibrium range of turbulence. Although these models cannot be directly derived from the Navier–Stokes equation, they offer a physically sound explanation for the Reynolds number dependence of $p_\varepsilon(\varepsilon)$ and its related quantities (e.g. skewness and flatness of $\partial u_i/\partial x_i$) and the anomalous scaling of inertial-range velocity structure functions (Frisch 1995). Historically, the (multi)fractal description of turbulence originates from the concept of the energy cascade of Richardson and Kolmogorov. In the view of the latter, the energy brought into the flow feeds into large eddies of characteristic size l_0 and characteristic velocity v_0, where l_0 is comparable to the integral length scale of the flow, and v_0 is understood as the velocity difference between two points separated by a distance l_0 which is comparable to the root-mean-square velocity of the flow. The motion of these large eddies is unstable which leads to the formation of somewhat smaller eddies of size l_1 and velocity v_1 which now receive their energy from their larger mother eddies. These smaller eddies are themselves unstable and form even smaller eddies of size l_2 and velocity v_2. This process continuous until the eddies reach a size where viscosity is effective in dissipating the energy that is cascading from the large to successively smaller eddies.

In (multi)fractal models, the Richardson–Kolmogorov eddy cascade is elaborated as a multiplicative random process. Basically, the length and the velocity of eddies of the nth generation are related to their mother eddies through $l_n = W l_{n-1}$ and $v_n = M v_{n-1}$, where M and W are random variables whose probability distribution is independent of n, i.e. of the length and velocity scale (we continue to use the term eddy to link the multiplicative process to the Kolmogorov–Richardson cascade; in the present context an eddy refers simply to a parcel of fluid). For illustration, let us consider two simple choices of M and W. In the β-model by Frisch, Sulem & Nelkin (1978) $W = 1/2$, and M is such that a fraction $\beta \leqslant 1$ of the 2^3 eddies formed at each cascade step have $M = (2\beta)^{-1/3}$ whereas the remaining eddies have $M = 0$. Accordingly, the cascade consists of eddies with finite velocity (active eddies) and eddies with zero velocity (passive eddies). As shown shortly, this choice of M and W leads to a fractal cascade. The other is the one-dimensional p-model of Meneveau & Sreenivasan (1987, 1991) where $W = 1/2$, and for the two eddies formed at each cascade step M assumes either a value P_1 or P_2, where energy conservation requires $P_1^3 + P_2^3 = 1$.

From these simple models it is seen that the fluctuations in v_n become stronger as n increases, i.e. as (l_n/l_0) decreases. It is convenient in the following to express the velocity scale at the nh generation through

$$v_l = v_0 \left(l/l_0\right)^h, \tag{3.1}$$

where, for simplicity, $v_l \equiv v_n$ and $l \equiv l_n$, and where the scaling exponent h is a random variable that fluctuates between limits that are independent of (l/l_0). Equation (3.1) is also the starting point of a more detailed interpretation of multifractal models (Frisch 1995) (where (3.1) is treated as a scaling relation instead of an equality) which is based on the observation that in the limit of zero viscosity (i.e. infinite Reynolds number and, accordingly, $(l/l_0) \to 0$) the Navier–Stokes equation is invariant under the scaling transformation $u^* = \lambda^h u$, $x^* = \lambda x$, $t^* = \lambda^{1-h} t$, where λ is a positive factor.

It is readily observed from our two simple cases of M and W that the fraction of fluid assuming a certain value of h depends on the number of generations in the cascade, that is, on (l/l_0). In the β-model where v_l is either finite in the active regions or zero in the passive regions, the fraction of fluid where h assumes a finite value is $(l/l_0)^{-\log_2 \beta}$. Generally, within a constant factor, the fraction of fluid assuming a value $(h, h + dh)$ is expressed through

$$p_h(h)dh \sim (l/l_0)^{d_s - f_h(h)}\, dh, \tag{3.2}$$

where d_s is the dimension of the space and $f_h(h)$ is a function that becomes scale invariant for $(l/l_0) \to 0$. From (3.2) it is seen that for $f_h(h) < d_s$ the fraction of fluid assuming a certain value of h is decreasing with decreasing (l/l_0) which allows us to interpret $f_h(h)$ as a fractal dimension. Accordingly, the function $f_h(h)$ is referred to as the multifractal spectrum.

The multifractal spectrum resulting from both the β-model and the p-model lead however to an inadequate description of the turbulent flow. In particular, the β-model leads to a linear relation for the scaling exponent of the velocity structure function in disagreement with experiments (Frisch 1995, p. 132). The p-model, on the other hand, which is developed assuming a one-dimensional cascade, covers only scaling exponents for which (in three dimensions) $f_h(h) > 2$, or, in other words, only eddies that fill the space with a fractal dimension larger than 2. Rare events that exhibit a small fractal dimension and which are found to be very violent (i.e. large values of v_l) are not described by the p-model. A better description is thus obtained by estimating $f_h(h)$ directly from experiments (Meneveau & Sreenivasan 1991) without assuming a model for M and W. Before referring to $f_h(h)$ determined from experiments, let us elaborate how the present results can be used to describe the PDF of the local energy dissipation rate.

Let us consider the cascade of successively smaller eddies from above. Following the refined similarity hypothesis (Kolmogorov 1962), the volume-averaged energy dissipation rate over an eddy of size l is $\varepsilon_l \sim v_l^3/l$ (Frisch *et al.* 1978). Hence, analogous to the characteristic eddy velocity v_l resulting from a multiplicative process, so does ε_l. Therefore, using $v_l \sim (\varepsilon_l l)^{1/3}$ in (3.1) and (3.2) we obtain

$$\varepsilon_l = \langle \varepsilon \rangle \, (l/l_0)^{\alpha - 1}, \tag{3.3}$$

and

$$p_\alpha(\alpha) \sim (l/l_0)^{d_s - f_\alpha(\alpha)}, \quad (l/l_0) \to 0, \tag{3.4}$$

respectively, where the scaling exponent $\alpha = 3h$ and $f_\alpha(\alpha) = f_h(\alpha/3)$, and where $\langle \varepsilon \rangle = v_0^3/l_0$. The cascade terminates when viscosity is effective in dissipating the energy brought into the flow. This happens at a length scale $l_d = (\nu^3/\varepsilon_l)^{1/4}$. Substituting this expression into (3.3) results in

$$\varepsilon = \langle \varepsilon \rangle \left(\frac{\eta}{l_0} \right)^{4(\alpha-1)/(\alpha+3)}. \tag{3.5}$$

Note that we do not to index the left hand side of (3.5), implying that the energy dissipation rate averaged over the dissipation scale $l_d = l_0 \, (\eta/l_0)^{4/(\alpha+3)}$ equals the local energy dissipation rate. The probability of having $\varepsilon \in (\varepsilon, \varepsilon + d\varepsilon)$ is given in the following by the probability of having a scaling exponent $\alpha \in (\alpha, \alpha + d\alpha)$ for an eddy of size l_d, which is given by (3.4). Substituting for l_d in (3.4) results in

$$P_\alpha(\alpha) \sim \left(\frac{\eta}{l_0} \right)^{4[d_s - f_\alpha(\alpha)]/(\alpha+3)}, \quad (\eta/l_0) \to 0 \tag{3.6}$$

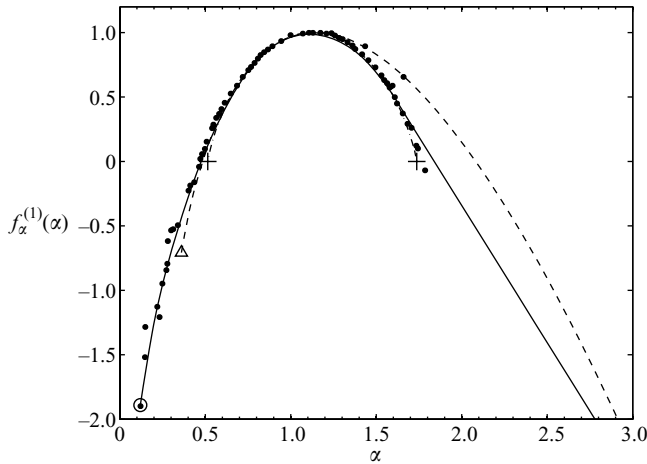FIGURE 3. One-dimensional multifractal spectrum $f_\alpha^{(1)}(\alpha)$. Solid symbols refer to measurements of Meneveau & Sreenivasan (1991). The curves refer to $f_\alpha^{(1)}(\alpha)$ given by (3.8) (solid curve), She & Leveque (1994) (dashed curve), and the *p*-model (dashed-dotted curve). For these models, the minimum value of α that characterizes the most violent turbulent events is $\alpha_{min} = 0.12$ ($\bigcirc$), 0.33 ($\triangle$) and 0.51 ($+$), respectively.

where a capital letter P is used to indicate that (3.6) refers to the dissipation length scale. From (3.6), the PDF of the local energy dissipation rate, $p_\varepsilon(\varepsilon)$, is obtained within a constant factor through

$$p_\varepsilon(\varepsilon)\mathrm{d}\varepsilon = P_\alpha(\alpha)\mathrm{d}\alpha. \tag{3.7}$$

3.1.2. *The multifractal spectrum*

Let us now turn to the multifractal spectrum $f_\alpha(\alpha)$. Figure 3 shows the one-dimensional spectrum, $f_\alpha^{(1)}(\alpha)$ (the superscript indicates that the embedded dimension of the spectrum is $d_s = 1$), determined experimentally (Meneveau & Sreenivasan 1991). Essentially, $f_\alpha^{(1)}(\alpha)$ is the logarithm of the PDF of α, whereas α itself is the negative logarithm of ε ((3.5) and (3.6)). Hence, small values of α refer to large values of ε, and vice versa. These assume small values of $f_\alpha^{(1)}(\alpha)$ and therefore appear with low probability.

The estimation of the spectrum deserves some comments. Meneveau & Sreenivasan (1991) determined $f_\alpha^{(1)}(\alpha)$ via the moments of ε_l. Thereby, high-order moments of ε_l that emphasize regions of intense dissipation were obtained by extrapolating the tails of the PDF of ε_l. This allowed them to estimate the left-hand tail of $f_\alpha^{(1)}(\alpha)$ shown in figure 3. Also, the infimum of α was estimated through this procedure as $\alpha_{min} = 0.12$ which is close to $\alpha_{min} = 0.15$ found by van de Water & Herweijer (1999) by evaluating high-order transverse velocity structure functions through a simple scaling argument (applying their scaling argument to longitudinal velocity structure functions leads to $\alpha_{min} = 0.48$). On the other hand, negative high-order moments of ε_l that accentuate regions of low dissipation were not calculated by Meneveau & Sreenivasan due to insufficient statistical convergence and no extrapolation was applied to obtain these moments. Hence, the right-hand tail of $f_\alpha^{(1)}(\alpha)$ shown in figure 3 where α assumes large values contains relatively few data points.
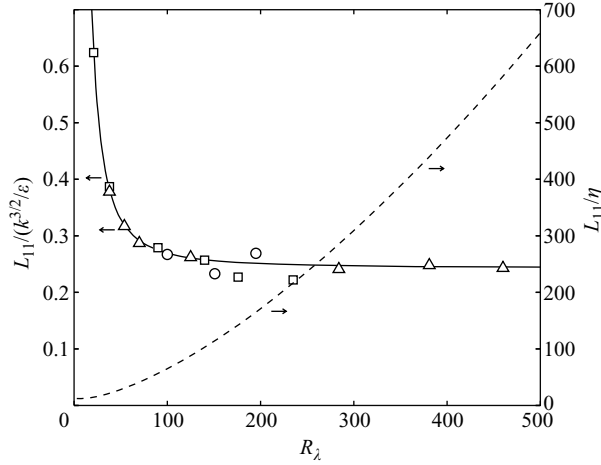
FIGURE 4. Length scale separation as a function of R_λ. The solid curve shows $L_{11}/\mathscr{L}$ given by (3.9) where $\mathscr{L} = k^{3/2}/\langle \varepsilon \rangle$. Symbols refer to numerical simulations: $\bigcirc$, Wang et al. (1996); $\square$, Vedula & Yeung (1999); $\triangle$, Gotoh, Fukayama & Nakano (2002). The dashed curve shows L_{11}/η given by (3.11).

The experimental spectrum is fitted through (Bałdyga & Podgórska 1998)

$$f_\alpha^{(1)}(\alpha) = \begin{cases} \sum_{i=0}^{8} a_i \alpha^i, & \alpha_{\min} \leqslant \alpha \leqslant b, \\ c_1 \alpha + c_0, & b < \alpha, \end{cases} \tag{3.8}$$

where $a_0 = -3.510$, $a_1 = 18.721$, $a_2 = -55.918$, $a_3 = 120.900$, $a_4 = -162.540$, $a_5 = 131.510$, $a_6 = -62.572$, $a_7 = 16.100$, $a_8 = -1.7264$, $b = 1.61$, $c_1 = -2.127$ and $c_0 = 3.913$ and which is shown by the solid curve in figure 3. Describing the right-hand tail of the spectrum ($\alpha > 1.61$) by a linear function is motivated by a comparison of the PDF of the local energy dissipation rate with that obtained from numerical simulations as discussed shortly. For completeness, figure 3 shows also $f_\alpha^{(1)}(\alpha)$ given by the p-model assuming $P_1^3 = 0.4$ and $P_2^3 = 0.6$ (Meneveau & Sreenivasan 1991) (dashed-dotted curve; to emphasize the limits of the p-model the limiting values of α that admit $f_\alpha^{(1)}(\alpha) = 0$ are indicated by $+$). Additionally, figure 3 shows $f_\alpha^{(1)}(\alpha)$ derived by She & Leveque (1994) (dashed curve) which was derived by relating the ratio of two adjacent integer moments of ε_l to some flow structures. Regarding the left-hand tail of $f_\alpha^{(1)}(\alpha)$, both the p-model and the model by She & Leveque give reasonable agreement with the measurements. A significant difference is however observed for the infimum of α where the p-model and the model by She & Leveque give $\alpha_{\min} = 0.51$ and 0.33, respectively, which are significantly larger than $\alpha_{\min} = 0.12$ found by Meneveau & Sreenivasan (1991). Bałdyga & Podgórska (1998) argue that $\alpha_{\min} = 0.12$ is more realistic since only such small values of $\alpha_{\min}$ can describe the asymptotic scaling of the maximum stable drop size with $\langle \varepsilon \rangle$ in liquid–liquid dispersions of fluids of similar viscosity.

Having established a functional form of the multifractal spectrum, the PDF of the local energy dissipation rate follows from (3.6) and (3.7), once the length scale separation (η/l_0) is fixed. The latter depends on the Reynolds number and it is this dependence that implies the Reynolds-number dependence of $p_\varepsilon(\varepsilon)$ in the multifractal model. A reasonable estimate for l_0 is the longitudinal integral length scale L_{11}. Figure 4 shows L_{11} normalized by $\mathscr{L} = k^{3/2}/\langle \varepsilon \rangle$ as a function of R_λ, where k is the

turbulent kinetic energy and R_λ is the Reynolds number based on the Taylor length scale. It is found that with increasing R_λ the normalized integral length scale relaxes to a constant value. The relaxation is fitted through

$$L_{11}/\mathscr{L} = b_1 + (b_2 + b_3 R_\lambda)^{b_4}, \qquad (3.9)$$

where $b_1 = 0.243$, $b_2 = 0.027$, $b_3 = 0.082$ and $b_4 = -1.727$. Expressing the Reynolds number through (Pope 2000, chap. 6)

$$R_\lambda = \left(\frac{20}{3}\frac{k^2}{\langle\varepsilon\rangle\nu}\right)^{1/2}, \qquad (3.10)$$

results finally in

$$l_0/\eta \approx \frac{L_{11}}{\eta} = \left(\frac{3}{20}R_\lambda^2\right)^{3/4}\frac{L_{11}}{\mathscr{L}}, \qquad (3.11)$$

which is shown by the dashed curve in figure 4.

Figure 5 compares $p_\varepsilon(\varepsilon)$ obtained from the multifractal model with results from direct numerical simulations. It shows $p_\varepsilon(\varepsilon)$ for $R_\lambda = 38$–680 where the solid symbols refer to the PDF reported by Vedula, Yeung & Fox (2001) and Yeung *et al.* (2006*a*). The latter were obtained by solving the incompressible Navier–Stokes equation using a pseudospectral method. The computational domain consisted of a periodic box discretized in up to 2048^3 grid points. Statistically stationary fluid motion was realized by large-scale forcing and time integration proceeded over several integral time scales. The abscissa in figure 5 shows ε in normalized form where μ and σ refer to the mean and the standard-deviation of $\ln(\varepsilon/\langle\varepsilon\rangle)$, respectively. For $R_\lambda = 38$–243 they are reported in Vedula *et al.* (2001) whereas for $R_\lambda = 680$, $\mu = -0.83$ and $\sigma = 1.616$. For $R_\lambda = 90$ and 141, the model based on (3.8) (solid curves) deviates from the simulations for large values of ε; for $R_\lambda = 38$ and 243 a similar deviation is weak or absent. This deviation might originate from an insufficient length scale separation (η/l_0). Recall that the multifractal model (3.6) requires $(\eta/l_0) \to 0$ in order for $f_\alpha^{(1)}(\alpha)$ to become scale invariant (for the five Reynolds number shown in figure 5 we have from (3.11) $\eta/l_0 = 22$, 56, 104, 227, and 1043, respectively). It is further seen that the left-hand tail decays approximately linearly in log–log coordinates which motivated us to extend $f_\alpha^{(1)}(\alpha)$ in (3.8) by a linear right-hand tail. The model by She & Leveque (dashed curves) predicts smaller probabilities for large values of ε and the distribution is negatively skewed. Further, the simulations show clearly the appearance of violent events that exceed the maximum value of ε predicted by She & Leveque (open triangles).

Finally, for $R_\lambda = 680$, the multifractal model based on (3.8) leads to a distribution that is close to log–normal (represented by the dotted curves). This is not surprising since for such a large Reynolds number the range of ε shown in figure 5 corresponds to $0.3 < \alpha < 2.4$. In this region, the left-hand tail of $f_\alpha^{(1)}(\alpha)$ is approximately parabolic. A parabolic multifractal spectrum results from the refined model of Kolmogorov (1962), which assumes that ε_l (and ε) has a log–normal distribution, and, hence, we observe a PDF that is log–normal in the core (the multifractal model deviates from log–normality for $Z = (\ln\varepsilon/\langle\varepsilon\rangle - \mu)/\sigma > 5$ which is not shown in figure 5; the probability of events that deviate from log–normality are however very low). The log–normal model implies, however, strong constraints on the scaling exponent of the velocity structure functions (Frisch 1995) which have not received experimental confirmation. Therefore, the log–normal model is not considered further (a comparison with the
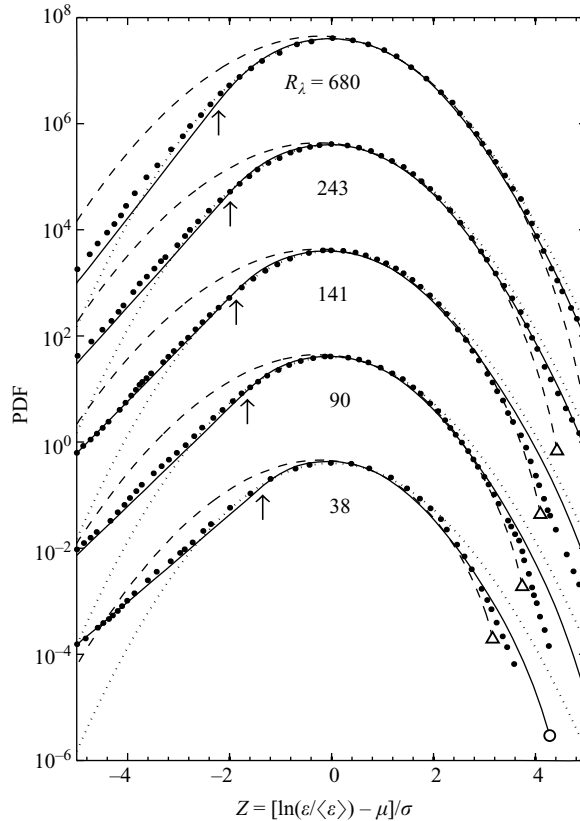
FIGURE 5. PDF of the local energy dissipation rate. Solid symbols refer to the PDF found by Vedula *et al.* (2001) and Yeung *et al.* (2006a). The solid and the dashed curves refer to the multifractal model with $f_\alpha^{(1)}(\alpha)$ given by (3.8) and by She & Leveque (1994), respectively. The maximum value of ε which are characterized by $\alpha_{\min}$ are indicated by $\bigcirc$ and $\triangle$ for the two models, respectively. The dotted curve represents the normal distribution. For convenience, the distributions for different R_λ are shifted upwards by a factor 10^2. The arrows mark the value of ε corresponding to $\alpha = 1.61$ above which $f_\alpha^{(1)}(\alpha)$ decays linearly.

scaling exponents of the velocity structure functions obtained experimentally and those resulting from $f_\alpha^{(1)}(\alpha)$ given by (3.8) is shown in Bäbler (2007, p. 168)).

To summarize, the PDF of the local energy dissipation rate follows from (3.7) where $\varepsilon(\alpha)$, $P_\alpha(\alpha)$, $f_\alpha^{(1)}(\alpha)$, and (η/l_0) are given by (3.5), (3.6), (3.8), and (3.11), respectively. The most violent turbulent events that assume $\varepsilon_{\max}$ are characterized by $\alpha_{\min} = 0.12$. For the subsequent integration of $p_\varepsilon(\varepsilon)$ it is convenient also to define a lower bound of ε, or, equivalently, an upper bound for α which is taken as $\alpha_{\max} = 3.0$. This is motivated by the observation that the decay of turbulence in any fluid element occurs with a finite rate and, hence, the local energy dissipation rate never vanishes (Borgas 1993). Further, based on the comparison of the multifractal model with direct numerical simulations (figure 5), the multifractal model is considered to be applicable for $l_0/\eta \geqslant 10$ or $R_\lambda \geqslant 10$.

3.2. *Time scale $\tau_\varepsilon(\varepsilon)$*

The time scale $\tau_\varepsilon(\varepsilon)$ gives the duration for which the flow in the vicinity of an aggregate persists. For a discussion it is therefore appropriate to switch to a Lagrangian frame

where we follow a particle that moves through the flow. Although considerable progress in obtaining Lagrangian statistics of particles in turbulence has been made recently, no statistical measure has been established to provide the duration of individual turbulent events. Thus, the present discussion aims to determine $\tau_\varepsilon(\varepsilon)$ from the Lagrangian autocorrelation of the energy dissipation rate.

Pope (1990) and Yeung, Pope & Sawford (2006*b*) obtained the latter by tracking the trajectories of fluid particles in a direct numerical simulation. A large range of Reynolds numbers was investigated. These data are applicable to the aggregates considered in this work, for which it is assumed that $R_p \ll 1$ and $St_p \ll 1$. The autocorrelation of ε was found to decay relatively fast at the beginning followed by a slow decay that persists for times of the order of the integral time scale (defined as the integral over the Lagrangian velocity autocorrelation function). The fast decay at the beginning scaled with the Kolmogorov time scale, $\tau_\eta = (\nu/\langle\varepsilon\rangle)^{1/2}$, independently of R_λ; the slow decay at $t \gg \tau_\eta$ was found to scale with the integral time scale. Hence, when scaled with τ_η the later part exhibited a R_λ-dependence such that the decay became slower with increasing R_λ. Plots of the energy dissipation rate along a particle trajectory are shown in Yeung (2001). The records show highly intermittent signals with intense but short-lived bursts appearing irregularly. The persistence of the slowly decaying tail in the autocorrelation function cannot therefore be interpreted as having few but long-living intense events. Instead, the slowly decaying tail is likely to be caused by a local crowding of short intense events along a particle trajectory. This view is supported in particular by the trapping of particles within vortical structures observed in experiments (La Porta *et al.* 2001) and simulations (Biferale *et al.* 2005; Yeung *et al.* 2007). Particles entrapped in such structures undergo helical ('corkscrew') motions with respect to a fixed frame of reference and are subject to strong but short pulses of centripetal acceleration (Biferale & Toschi 2005). The characteristic frequency of these helical motions is $O(\tau_\eta^{-1})$ and the trapping can last for as long as $10\tau_\eta$. Acceleration of a moving fluid particle is essentially caused by the velocity gradient of the surrounding fluid; it is related to the local energy dissipation rate via $\varepsilon = 2\nu s_{ij} s_{ij}$, where $s_{ij} = \frac{1}{2}(\partial u_i/\partial x_j + \partial u_j/\partial x_i)$ is the local rate of strain. Hence, the short pulses of acceleration within the vertical structures correspond to short pulses of high velocity gradients, and consequently to a high energy dissipation rate.

The shortness of the intense events is further supported by the autocorrelation functions of the individual components of the velocity gradient tensor (Yeung 2001). These decay relatively fast; the integral correlation time was found to be independent of R_λ and 2 to 6 times τ_η depending on the particular component . Thus, any directional information, and hence, the persistence of the flow in the vicinity of a particle, is rapidly lost (note that by a 'turbulent event' we strictly refer to the appearance of a certain value of the local energy dissipation rate).

The scaling of the autocorrelation function of ε with τ_η at short times suggests that the duration of a turbulent event is governed by local interactions whereas non-local interactions cause a crowding of events through vortical structures. Accordingly, $\tau_\varepsilon(\varepsilon)$ is taken to be proportional to the *local* Kolmogorov time scale,

$$\tau_\varepsilon(\varepsilon) = c^{-1} (\nu/\varepsilon)^{1/2}, \qquad (3.12)$$

where c is a positive factor. Taking (3.12) instead of $\tau_\varepsilon(\varepsilon) \sim \tau_\eta$ is motivated in particular by numerical measurements of the acceleration autocorrelation function conditioned on ε (Yeung *et al.* 2007). This is rapidly decaying and the decay is faster the larger ε upon which the correlation function is conditioned. From the fast decay of the Langrangian autocorrelations of ε, $\partial u_i/\partial x_j$, and the acceleration we conclude that

the factor $c \sim O(1)$. Finally, note that the time scale given in (3.12) was also used in the droplet breakup model of Bałdyga & Podgórska (1998).

4. Aggregate response function

This section treats the aggregate response function $\varepsilon_{cr}(x)$ that provides the boundaries of the integrals in the breakup rate function (2.7). Basically, we are interested in the response of an aggregate to an applied hydrodynamic stress generated by a flow of energy dissipation rate magnitude ε. Throughout this section, it is therefore convenient to express the aggregate response function through its inverse $x_{cr}(\varepsilon)$, where x_{cr} is the critical aggregate mass above which breakup occurs in a flow of magnitude ε. Experimental (Sonntag & Russel 1986) and numerical studies (Higashitani *et al.* 2001) suggest that $x_{cr}(\varepsilon)$ assumes a power law relationship,

$$x_{cr} = C_s \varepsilon^{-q}, \tag{4.1}$$

where C_s and q are positive parameters. A rationale for (4.1) is given by Zaccone *et al.* (2007). Assuming an aggregate behaves linearly elastically to the point of breakup they developed a model where C_s reduces to a parameter expressing the bond strength between the primary particles in the aggregate. The exponent q, on the other hand, depends on the packing of the primary particles, that is, on the aggregate structure. The present discussion focuses on the exponent q.

4.1. *Scaling approaches*

Aggregates smaller than the Kolmogorov length scale are subject to a hydrodynamic stress $\tau_f \sim \mu (\varepsilon/\nu)^{1/2}$ where ε (and therefore the local velocity gradient) is constant on the length scale of the aggregate. In order to withstand this stress the aggregate strength τ_a has to be larger than τ_f. Tomi & Bagster (1978) considered the aggregate strength to be a property of the aggregated material which is independent of the aggregate size. Since the hydrodynamic stress below the Kolmogorov length scale was also independent of the aggregate size, the aggregates break independently of their size once the hydrodynamic stress (i.e. the local energy dissipation rate) exceeds τ_a (i.e. a critical energy dissipation rate). In regard of the breakup model introduced in this work, this translates into $\varepsilon_{cr}(x) = \text{constant}$, which results in a constant breakup rate function. This is, however, infeasible as discussed in the context of (1.2).

Note however that a constant aggregate strength does not take into account the fractal structure of the aggregates. It is well known that the aggregation of small particles leads to structures that fill the space as a fractal (Lin *et al.* 1989). The mass of an aggregate then exhibits the following scaling with its size:

$$x \sim a^{d_f} \tag{4.2}$$

where d_f is the mass fractal dimension of an aggregate. Kusters (1991) assumed that the aggregate strength is a function of the local solid volume fraction, $\varphi(\mathbf{r})$, that is written as $\tau_a \sim \varphi(\mathbf{r})^n$, where $\mathbf{r}$ refers to the spatial position inside the aggregate with $\mathbf{r} = 0$ at the centre of mass of the aggregate. The exponent n is a parameter depending on the number of contacts among the primary particles in the aggregate. From (4.2), the local solid volume fraction is estimated as $\varphi(r) \sim r^{d_f-3}$, where $r = |\mathbf{r}|$, from which the aggregate strength follows as $\tau_a \sim a^{n(d_f-3)}$ (Kusters 1991; Bałdyga & Bourne 1995). Balancing τ_a with τ_f results in (Potanin 1993)

$$a_{cr} \sim \varepsilon^{-p}, \quad p = 1/[2n(3 - d_f)], \tag{4.3}$$

where a_{cr} is the critical aggregate size above which breakup occurs. Substituting the left-hand side of (4.3) into (4.2), we obtain

$$x_{cr} \sim \varepsilon^{-q}, \quad q = d_f/[2n(3 - d_f)]. \tag{4.4}$$

A more detailed analysis by Sonntag & Russel (1987b) using a power-law dependence of the elastic shear modulus on the local solid volume fraction and modelling the aggregate as a permeable sphere results in

$$p = (d_f - 1)/[4n(3 - d_f)], \quad q = d_f p, \tag{4.5}$$

which leads to slightly smaller values than (4.3) and (4.4). Measurements of the elastic shear modulus for space-filling networks (Sonntag & Russel 1987a) gave $n \approx 2.5 - 4.4$.

Equations (4.4) and (4.5) predict a strong dependence of the exponent q on d_f, and for $d_f \to 3$, i.e. for uniformly packed aggregates, the exponent q diverges and the critical aggregate size drops to zero above a critical energy dissipation rate, which reflects the situation of a size-independent aggregate strength. These findings are in qualitative agreement with the results of Horwatt *et al.* (1992a,b) who investigated the breakup of computer-generated aggregates. They found that with increasing fractal dimension, the breakup exponent q increases while at the same time the scatter in q as a function of d_f increases. The latter observation is explained by the increasing importance of flaws due to structure irregularities that become more pronounced as the aggregate becomes more dense (i.e. as d_f increases).

Potanin (1993) points out that the scaling analysis given above holds for colloidal bonds that exhibit angular rigidity which enables the stress acting on an aggregate to be transmitted to the structure (West, Melrose & Ball 1994). For bonds that exhibit no angular rigidity, i.e. no resistance to a tangential force, Potanin derived $p = 1/4$ through a simple force balance (Kobayashi *et al.* 1999). In this model the total hydrodynamic force acting on an aggregate, $F_f \sim \tau_f a^2$, is balanced by a force holding the aggregate together. Assuming the latter is constant, i.e. independent of the aggregate size, results in $a \sim \tau_f^{-1/2} \sim \varepsilon^{-1/4}$. This latter exponent ($p = 1/4$) is the typical value found in experiments for the scaling of a mean aggregate size at steady state (Selomulya *et al.* 2002; Coufort, Bouyer & Liné 2005; Kusters, Wijers & Thoenes 1997). Computer simulations of non-rigid aggregates confirm this result, e.g. Higashitani *et al.* (2001) considered radial interactions between the primary particles and a tangential resistance was only implemented for particles at contact. For aggregates with $d_f = 1.7$–2.5 it was found that in simple shear $p \approx 0.2$ which is close to $p \approx 0.24$ for $d_f = 1.9$ found by Harada *et al.* (2006). It is important however to notice the difference with breakup in extensional flow for which Higashitani *et al.* (2001) found p to be twice as large.

In summary, the aggregate response function is given (through its inverse) by (4.1), where the parameters C_s and q are assumed to depend on the aggregate properties, e.g. d_f. In order to have a non-dimensional form, it is convenient to introduce a reference mass x_0 that is defined as the mass of the largest aggregate that can survive in a turbulent event of magnitude $\langle \varepsilon \rangle$. The aggregate response function then becomes

$$x_{cr} = x_0(\varepsilon/\langle \varepsilon \rangle)^{-q}, \quad x_0 = C_s \langle \varepsilon \rangle^{-q}, \tag{4.6}$$

which is the form used in the following sections.

4.2. *Instantaneous breakup*

Let us finally turn to the assumption of instantaneous breakup for which experiments and simulations that are currently available provide only an indication: Blaser (2000)

investigated the breakup of aggregates in a flow through an orifice, and the sequences of images of the breaking aggregates shown in the paper allows us to conclude that breakup is fast. In a similar study by Sonntag & Russel (1987c), it was pointed out that for the flow through an orifice the duration over which the stress peaks is short. The study of Yeung & Pelton (1996) suggests that polymeric aggregates are brittle and, therefore, they break instantaneously once the stress exceeds a critical stress. More information is gained from simulations: those of Higashitani *et al.* (2001) where the bonds show partial rigidity only at contact gave a characteristic time for the breakup event of $\sim 10G^{-1}$ in simple shear, and $\sim G^{-1}$ in extensional flow. Potanin's (1993) simulations with bonds that exhibit partial rigidity suggest that breakup in simple shear takes $\sim G^{-1}$ which indicates that an essential factor that determines the dynamics of the breakup event is the rigidity of the bonds between the primary particles. In particular, it is expected that an aggregate whose bonds are non-rigid will exhibit a longer characteristic time for the breakup event.

5. Results

In this section we present an explicit expression for the breakup rate function resulting from the general expression given by (2.7). Further, we explore the breakup rate function that results from a Gaussian velocity gradient. Finally, we investigate the kinetics of a pure breakup process which is described by (1.1).

5.1. *Explicit expression for $K_B(x)$*

A key factor in the breakup rate function given by (2.7) is the PDF of the local energy dissipation rate, from which it is observed that ε is bounded (i.e. ε fluctuates between $\varepsilon_{\min}$ and $\varepsilon_{\max}$). In the multifractal model, the local energy dissipation rate is mapped by a scaling exponent α through (3.5). The most violent turbulent events that exhibit $\varepsilon_{\max}$ are characterized by $\alpha_{\min} = 0.12$. The critical aggregate mass corresponding to these events is denoted as x_L and from (3.5) and (4.6) is given by

$$x_L = x_0 \left(\frac{\eta}{l_0} \right)^{-4q(\alpha_{\min}-1)/(\alpha_{\min}+3)}. \tag{5.1}$$

Since there are no turbulent events violent enough to break aggregates smaller than x_L we have $K_B(x) = 0$ for $x \leqslant x_L$, which is a direct consequence of the fact that ε is bounded. On the other hand, the weakest turbulent events that exhibit $\varepsilon_{\min}$ are characterized by $\alpha_{\max} = 3.0$. The critical aggregate mass corresponding to these events is denoted as x_R and is given by (5.1), where $\alpha_{\min}$ is substituted for $\alpha_{\max}$. Aggregates larger than x_R are broken up by any turbulent event and therefore cannot exist. Hence, $K_B(x) \to \infty$ for $x > x_R$. From these considerations, it is recognized that only aggregates in the range $x_L < x < x_R$ are subject to breakup with a finite rate. The width of this range increases with increasing q and with increasing l_0/η, that is to say, with increasing Reynolds number. Figure 6 summarizes these findings by means of the aggregate response function $\varepsilon_{cr}(x)$. Table 1 lists x_L and x_R for typical values of l_0/η and q.

The mapping of the local energy dissipation rate by the scaling exponent α motivates us further to substitute the integration variable in (2.7) for α. Using (3.7) for $p_\varepsilon(\varepsilon)$ and expressing the time scale $\tau_\varepsilon(\varepsilon)$ through (3.12), the breakup rate function becomes

$$K_B(x) = c \left(\frac{\langle \varepsilon \rangle}{\nu} \right)^{1/2} \left[\int_{\alpha_{\min}}^{\alpha_{cr}(x)} P_\alpha(\alpha) \left(\frac{\varepsilon(\alpha)}{\langle \varepsilon \rangle} \right)^{1/2} d\alpha \right] \left[\int_{\alpha_{cr}(x)}^{\alpha_{\max}} P_\alpha(\alpha) \, d\alpha \right]^{-1} \tag{5.2}$$

	$l_0/\eta = 100$ $(R_\lambda \approx 137)$		$l_0/\eta = 1000$ $(R_\lambda \approx 660)$	
$\varepsilon_{max}/\langle\varepsilon\rangle$	1.8×10^2		2.4×10^3	
$\varepsilon_{min}/\langle\varepsilon\rangle$	2.2×10^{-3}		10^{-4}	
q	x_L/x_0	x_R/x_0	x_L/x_0	x_R/x_0
0.5	7.4×10^{-2}	2.2×10^1	2×10^{-2}	10^2
1.0	5.5×10^{-3}	4.6×10^2	4.1×10^{-4}	10^4
1.5	4.1×10^{-4}	10^4	8.4×10^{-6}	10^6

TABLE 1. Critical aggregate masses.
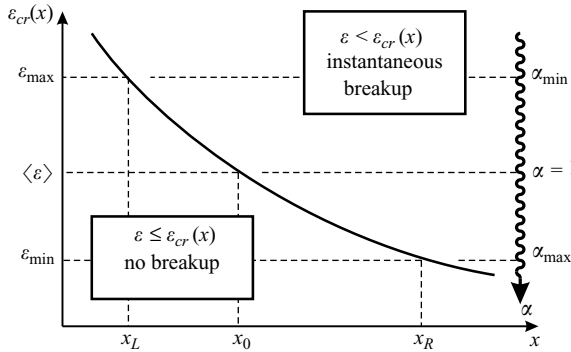
FIGURE 6. Aggregates in the range $x_L < x < x_R$ are subject to breakup with a finite rate. x_L and x_R are thereby determined by the most violent and the weakest turbulent events which are characterized by α_{min} and α_{max}, respectively.

where $\varepsilon(\alpha)$ and $P_\alpha(\alpha)$ are given by (3.5) and (3.6), respectively, and $\alpha_{cr}(x)$ corresponds to $\varepsilon_{cr}(x)$ which follows from (4.6) as

$$\alpha_{cr}(x) = \frac{3J + 4}{4 - J}, \quad J = \frac{1}{q}\frac{\ln x/x_0}{\ln l_0/\eta}, \quad x_L < x < x_R. \tag{5.3}$$

Explicit expressions for the FMDs ((2.11) and (2.13)), are obtained in a similar way which is not described further.

Figure 7 shows the breakup rate function given by (5.2) as a function of x/x_0 for four pairs of values of q and the length scale separation l_0/η, where the latter enters (5.2) through $P_\alpha(\alpha)$. As deduced above, $K_B(x)$ vanishes for $x \to x_L$ and diverges for $x \to x_R$ where x_L (x_R) decreases (increases) with increasing q and l_0/η. In the normalized coordinates shown in figure 7, the dependence of $K_B(x)$ on l_0/η appears weak. This means that an increase of R_λ, which implies an increase of l_0/η, changes the shape of $K_B(x)$ only slightly; its position and its magnitude changes with x_0 and τ_η which are both decreasing with increasing R_λ. The change in the shape of $K_B(x)$ with increasing R_λ has a significant influence on the scaling of the asymptotic aggregate size however, as shown below. For a fixed value of l_0/η, the curves at different values of q cross at $x/x_0 = 1$, which is due to the fact that for $x = x_0$, we have $\alpha_{cr}(x) = 1$, and the numerator and denominator in (5.2) become independent of q. Regarding the dependence on l_0/η it is found that $K_B(x)$ at $x = x_0$ is weakly dependent, and for $l_0/\eta = 100$ and 1000 we have $K_B(x_0)c/\tau_\eta = 0.552$ and 0.516, respectively.
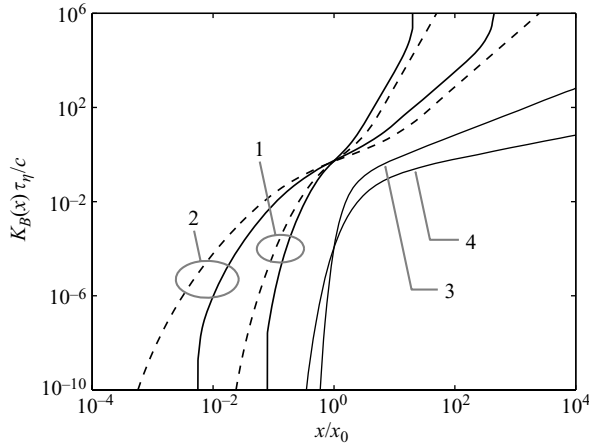
FIGURE 7. Breakup rate function given by (5.2) (curves 1 and 2) and (5.7) (curves 3 and 4). For 1 and 2 solid and dashed lines refer to $l_0/\eta = 100$ and 1000 respectively. Curves 1 and 3 have $q = 0.5$ and curves 2 and 4 have $q = 1.0$.
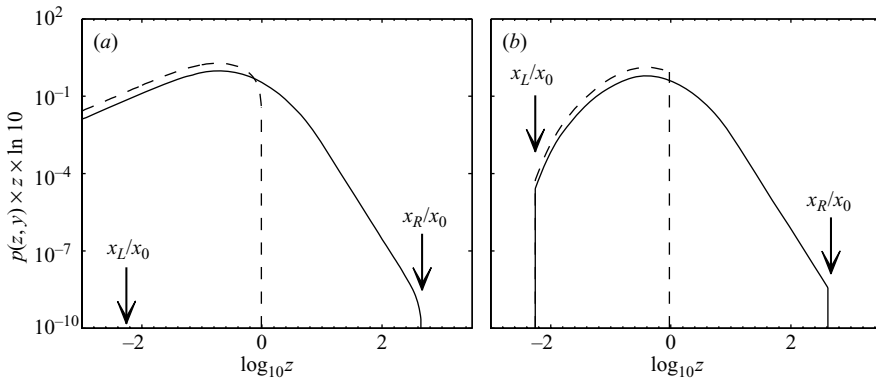

FIGURE 8. FMD based on a (*a*) uniform elementary FMD and a (*b*) Dirac elementary FMD for $q = 1.0$ and $l_0/\eta = 100$. The solid curves refer to the FMD for $y \geqslant x_R$ and the dashed curves to $y = x_0$. On the axis, $z = x/x_0$ and $p(z, y) = g(x, y)x/y$.

The FMDs resulting from (2.11) and (2.13) are shown in figure 8 as a function of the normalized aggregate mass $z = x/x_0$. It is observed that the FMD based on a uniform elementary FMD (figure 8*a*, (2.11)) leads to a large number of small fragments. On the other hand, the smallest fragments formed by the FMD based on a Dirac elementary FMD (figure 8*b*, (2.13)) have a mass equal to x_L. It is further seen that the position of the FMD is determined by x_0. The mass of the breaking aggregate, y, determines solely the right-hand boundary of the FMD. This becomes clear by comparing the solid and the dashed curves that refer to $g(x, y)$ for $y \geqslant x_R$ and $y = x_0$, respectively. It is this behaviour that demontrates the FMDs given by (2.11) and (2.13) to be non-self-similar with respect to the mass ratio x/y.

5.2. $K_B(x)$ based on a Gaussian velocity gradient

An alternative formulation of the breakup rate function is obtained by considering the characteristic local velocity gradient, $\gamma \sim \varepsilon^{1/2}$, as the fluctuating quantity that induces breakup instead of the local energy dissipation rate. Since γ can be either

positive or negative, the equivalent expression to (2.7) in this case is

$$K_B(x) = \frac{\int_{|\gamma| > \gamma_{cr}(x)} p_\gamma(\gamma)/\tau(\gamma)\,\mathrm{d}\gamma}{\int_{|\gamma| \leqslant \gamma_{cr}(x)} p_\gamma(\gamma)\,\mathrm{d}\gamma}, \tag{5.4}$$

where $p_\gamma(\gamma)$ and $\tau_\gamma(\gamma)$ are the PDF and the characteristic time of the local velocity gradient, respectively, and $\gamma_{cr}(x)$ is the critical velocity gradient above which an aggregate of mass x breaks up. To proceed, let us assume γ to be given by the local longitudinal velocity gradient, $(\partial u_i/\partial x_i)$, and let us approximate the PDF of γ to be Gaussian (Saffman & Turner 1956) with zero mean and a variance equal to

$$\sigma^2 = \left\langle \left(\frac{\partial u_i}{\partial x_i}\right)^2 \right\rangle = \frac{1}{15}\frac{\langle \varepsilon \rangle}{\nu}. \tag{5.5}$$

It has to be emphasized that this is a severe assumption, and $(\partial u_i/\partial x_i)$ deviates significantly from being Gaussian. In particular, the PDF of $(\partial u_i/\partial x_i)$ is negatively skewed (Sreenivasan & Antonia 1997) and the tails are wider than Gaussian (Castaing, Gagne & Hopfinger 1990; Kailasnath, Sreenivasan & Stolovitzky 1992; Sreenivasan 1999). However, as shown shortly, this assumption leads to a breakup rate function that in the limit of very small and very large aggregates reduces to an exponential function and a power law that are formally identical to (1.2) and (1.3), respectively. This demonstrates the strength of the present model in interpretting the existing rate expressions.

The remaining functions in (5.4) are described in accordance with (5.2). That is, the characteristic time of the velocity gradient is taken as $\tau(\gamma) = (c'\gamma)^{-1}$, where $c' \approx c$, and the aggregate response function is $x_{cr} = C_s'\gamma^{-2q}$, where (using $\gamma \approx (\varepsilon/\nu)^{1/2}$) $C_s' \approx C_s\nu^{-q}$. As above, it is convenient to introduce a reference mass x_0', such that

$$x_{cr} = x_0'(\gamma/G)^{-2q}, \quad x_0' = C_s'G^{-2q}. \tag{5.6}$$

Substitution into (5.4) results in

$$K_B(x) = \frac{2c'\sigma}{\sqrt{2\pi}}\frac{\exp(-X^2)}{\mathrm{erf}(X)} = c'\sqrt{\frac{2}{15\pi}}\left(\frac{\langle \varepsilon \rangle}{\nu}\right)^{1/2}\frac{\exp(-X^2)}{\mathrm{erf}(X)}, \tag{5.7}$$

where $\mathrm{erf}(.)$ is the error function, and

$$X = \frac{\gamma_{cr}(x)}{\sqrt{2}\,\sigma} = \sqrt{\frac{15}{2}}\left(\frac{x}{x_0'}\right)^{-1/(2q)} = \sqrt{\frac{15}{2}}\left(\frac{\langle \varepsilon \rangle}{\nu}\right)^{-1/2}\left(\frac{x}{C_s'}\right)^{-1/(2q)}. \tag{5.8}$$

Curve 3 and 4 in figure 7 show $K_B(x)$ given by (5.7) as a function of (x/x_0') for $q = 0.5$ and 1.0, respectively (axis labels x_0 and c should be read as x_0' and c', respectively). It is observed that $K_B(x)$ exhibits a strong dependence on x for (x/x_0') around unity, and that it falls off rapidly with decreasing x. This reflects the narrowness of the Gaussian PDF which causes aggregates smaller than x_0' to exhibit very slow breakup rates. On the other hand, for $x \gg x_0'$ $K_B(x)$ increases linearly in log–log coordinates where the slope is decreasing with increasing q.

From (5.7), it is seen that for $x \ll x_0'$ we have $X \gg 1$ and $\mathrm{erf}(X) \to 1$, and (5.7) reduces to (1.2) with the difference in c' that according to the derivation of Kusters (1991) $c' = \sqrt{2}$. Flesch *et al.* (1999) proposed further that $q = d_f$ (i.e. the critical aggregate size above which breakup occurs is assumed to scale as $a_{cr} \sim \gamma^{-2}$) which

leads to $X^2 \sim a^{-1}$ for the argument of the exponential. On the other hand, for $x \gg x'_0$ it follows that $X \ll 1$ and noting that $\text{erf}(X) = X$ for $X \to 0$ (5.7) reduces to

$$K_B(x) = \frac{c'}{\sqrt{30}} \left(\frac{\langle \varepsilon \rangle}{\nu} \right)^{1/2} X^{-1} = c' \sqrt{\frac{2}{450}} \frac{\langle \varepsilon \rangle}{\nu} \left(\frac{x}{C'_s} \right)^{1/(2q)}, \quad x \gg x'_0, \qquad (5.9)$$

which is recognized as a power-law breakup rate function. Hence, the assumption of a Gaussian velocity gradient allows as to recover both (1.2) and (1.3).

The simple form of $p_\gamma(\gamma)$ allows us also to derive explicit expressions for the global FMDs. In the case of a uniform elementary FMD, from (2.11) the global FMD equates to

$$g(x, y) = 2 \left(\frac{2}{15} \right)^{2q} \left(\frac{y}{x_0^2} \right) \frac{\Gamma(2q+1, Y^2) - \Gamma(2q+1, X^2)}{\exp(-Y^2)}, \quad x \leqslant y, \qquad (5.10)$$

where Γ is the upper incomplete gamma function, and Y is given by (5.8) by substituting x for y. In the case of a Dirac elementary FMD, from (2.13) we have

$$g(x, y) = \frac{1}{q} \left(\frac{y}{x^2} \right) \frac{X^2 \exp(-X^2)}{\exp(-Y^2)}, \quad x \leqslant y. \qquad (5.11)$$

The FMDs given by (5.10) and (5.11) (not shown) are qualitatively similar to the FMDs resulting from the multifractal model shown in figure 8, with the difference in the formation of large fragments: the FMDs resulting from the Gaussian model produce fragments in the range $(0, y)$ while in the multifractal model the largest fragments have a mass equal to x_R.

5.3. *Breakup kinetics*

Breakup kinetics are investigated in two parts. In the first part we remain with non-dimensional variables and focus on the evolution of the CMD and on the influence of the FMD. In the second part, we consider a specific flow and investigate the scaling of the mean aggregate size with the Reynolds number.

5.3.1. *Time evolution of the CMD*

Let us consider a monodisperse suspension of aggregates of mass x_0 undergoing breakup. The time evolution of the CMD is described by (1.1) subject to

$$t = 0: \quad c(x, t) = C_0 \delta(x - x_0), \qquad (5.12)$$

where C_0 is the initial number of aggregates. The breakup rate function and the FMD are given by (5.2), (2.11) or (2.13), respectively. Equation (1.1) is solved numerically using the discretization scheme developed by Kumar and Ramkrishna (see Bäbler 2007, §2).

Figure 9 shows the time evolution of the mean aggregate mass $\bar{x}$ (solid curve) and a mass-weighted mean aggregate mass I_0 (dashed curve) for a uniform elementary FMD (curve 1) and a Dirac elementary FMD (curve 2). Here, $\bar{x}$ and I_0 are defined as

$$\bar{x} = \frac{\int_0^\infty c(x, t) x \, \mathrm{d}x}{\int_0^\infty c(x, t) \, \mathrm{d}x}, \quad I_0 = \frac{\int_0^\infty c(x, t) x^2 \, \mathrm{d}x}{\int_0^\infty c(x, t) x \, \mathrm{d}x}. \qquad (5.13)$$

I_0 is experimentally accessible through static light scattering where the mass-weighted mean aggregate mass is proportional to the scattering intensity at zero scattering angle
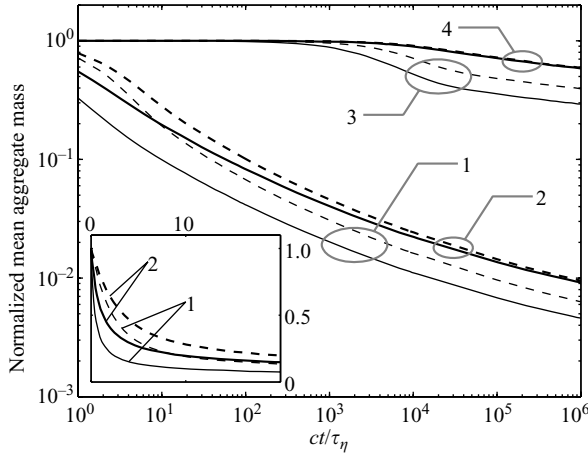
FIGURE 9. Time evolution of the mean aggregate mass (solid curves) and the mass-weighted mean aggregate mass (dashed curves) resulting from the breakup of a monodisperse distribution of aggregates of mass x_0. The ordinate is normalized by the reference mass x_0. Curves 1 (uniform elementary FMD) and 2 (Dirac elementary FMD) refer to the multifractal model where $q = 1.0$ and $l_0/\eta = 100$. Curves 3 (uniform elementary FMD) and 4 (Dirac elementary FMD) refer to the Gaussian model where $q = 1.0$. The inset shows the initial decay in linear coordinates for the multifractal model.

(explaining the meaning of the symbol I_0). The ordinate in figure 9 is normalized by x_0, and the abscissa is plotted in log-coordinates which reveals the transient decay of the mean aggregate size. It is seen that the FMD has little influence on the evolution of the mean aggregate size. The Dirac elementary FMD (curve 2) leads to a mean aggregate size that is only slightly larger that one resulting from a uniform elementary FMD (curve 1). For the latter, the asymptotic values for $\bar{x}$ and I_0 are $\frac{1}{2}x_L$ and $\frac{2}{3}x_L$, respectively. For a Dirac FMD both $\bar{x}$ and I_0 converge to x_L, which in the present case equates to $x_L/x_0 = 5.5 \times 10^{-3}$. Curves 3 and 4 in figure 9 show additionally the time evolution of $\bar{x}$ and I_0 resulting from the Gaussian model, that is, $K_B(x)$ given by (5.7) and $g(x, y)$ given by (5.10) (curve 3) or (5.11) (curve 4), respectively. In this case the decay of the mean aggregate mass is significantly slower, and at $ct/\tau_\eta = 10^6$ we have $\bar{x}/x_0 = 0.29$ and 0.58 for the uniform and the Dirac elementary FMD, respectively.

The evolution of the CMD resulting from the multifractal model is shown in figure 10. In the case of a uniform elementary FMD (figure 10a) fragments of all sizes are produced in the first instance, and fragments larger than x_L are consumed in the course of the process, shifting the CMD to the left. For $t \to \infty$ the CMD for the considered FMD is

$$c(x, \infty) = \begin{cases} c_\infty, & x \leqslant x_L \\ 0, & \text{otherwise,} \end{cases} \tag{5.14}$$

where $c_\infty = 2C_0 x_0/x_L^2$. In the case of a Dirac elementary FMD (figure 10b) in the first instance breakup produces only fragments in the range $x_L < x < x_0$, and the larger fragments are consumed in the course of the process. For $t \to \infty$, the CMD converges to a monodisperse distribution,

$$c(x, \infty) = C_\infty \delta(x - x_L), \tag{5.15}$$

where $C_\infty = C_0 x_0/x_L$. It is further seen that in this case $\bar{x}$ and I_0, shown by the filled and open symbols in figure 10, respectively, assume very similar values except at

N (rpm)	ε_{av} (m^2 s^{-3})	k_{av} (cm^2 s^{-2})	τ_η (10^{-3} s)	η (μm)	R_λ (−)	l_0/η (−)
200	0.0304	27	5.74	76	40	22
417	0.268	123	1.93	44	61	35
635	0.932	294	1.04	32	79	47
854	2.24	542	0.67	26	94	59
1073	4.40	870	0.48	22	107	71

TABLE 2. Characteristics of the turbulent flow.
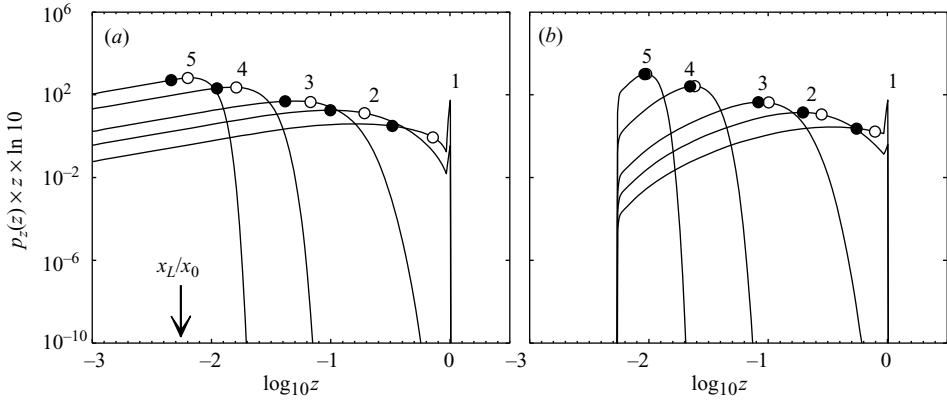
FIGURE 10. CMD resulting from the breakup of a monodisperse distribution of aggregates of mass x_0 using (*a*) a uniform elementary FMD and (*b*) a Dirac elementary FMD. $q = 1.0$ and $l_0/\eta = 100$, and curves 1–5 refer to $ct/\tau_\eta = 1$, 10, 10^2, 10^4, and 10^6, respectively. On the axis, $z = x/x_0$ and $p_z(z) = c(x)/C_0$ where C_0 is the initial number of aggregates. Solid and open symbols indicate the mean aggregate mass and the mass-weighted mean aggregate mass, respectively.

the very beginning. The Gaussian model (not shown) leads to a qualitatively similar behaviour which is not discussed further.

5.3.2. *Scaling of the asymptotic mean aggregate size*

To investigate the asymptotic scaling of the mean aggregate size let us consider a specific case: Soos *et al.* (2008) studied the aggregation of polystyrene particles in a stirred tank. The radius of the primary particles was $a_p = 0.405\,\mu\text{m}$ and the particles were fully destabilized. The characteristics of the turbulent flow in the stirred tank used in this study are listed in table 2, where the subscript 'av' refers to volume averages of the stirred tank and N is the stirring speed. For simplicity, in the subsequent analysis the flow is treated as homogeneous, and ε_{av} and k_{av} are interpreted as the mean values of the flow. To proceed, (1.1) with the initial condition given by (5.12) is solved for the five sets of parameters listed in table 2 assuming a uniform elementary FMD. Figure 11 shows the asymptotic values of the mean aggregate mass (figure 11*a*) and the mean radius of gyration (figure 11*b*) as a function of $\langle\varepsilon\rangle$. The non-dimensional
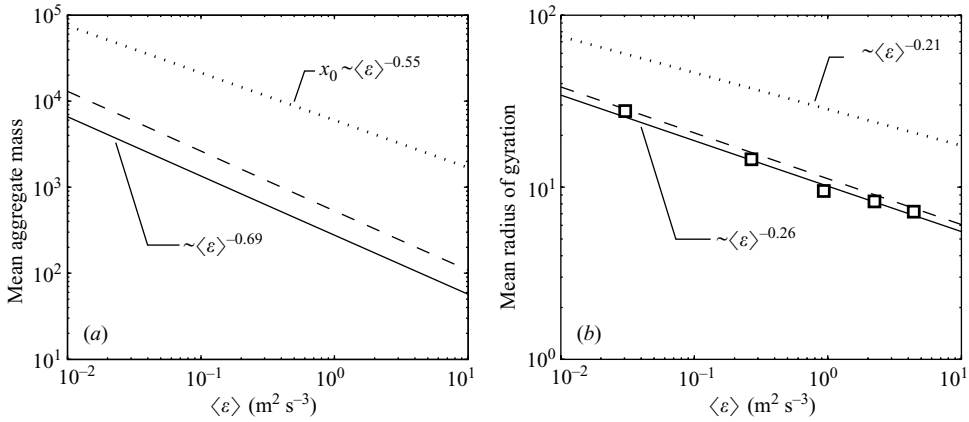
FIGURE 11. Asymptotic values of the mean aggregate mass (*a*) and the mean radius of gyration (*b*) as a function of $\langle\varepsilon\rangle$ calculated assuming a uniform elementary FMD. The solid lines in (*a*) and (*b*) refer to the asymptotic values of $\bar{x}$ and ρ, respectively. The dashed and the dotted lines in (*a*) refer to x_L and x_0, respectively, while in (*b*) they refer to the corresponding aggregate sizes x_L^{1/d_f} and x_0^{1/d_f}, respectively. The open symbols in (*b*) refer to the experimental values reported in Soos *et al.* (2008).

mean radius of gyration is given by (Lattuada *et al.* 2003)

$$
\rho = \left[\frac{\int_0^\infty c(x,t)x^2(R_g(x)/a_p)^2\,\mathrm{d}x}{\int_0^\infty c(x,t)x^2\,\mathrm{d}x} \right]^{1/2}, \tag{5.16}
$$

where $R_g(x) = a_p x^{1/d_f}$ is the radius of gyration of an aggregate of mass x, whereas $d_f = 2.6$ was assumed (Soos *et al.* 2008). The reference mass $x_0 = C_s\langle\varepsilon\rangle^{-q}$, where $C_s = 6 \times 10^3$ (m^2 s^{-3})^q, and $q = 0.55$ was selected such that the asymptotic mean radius of gyration resulting from the simulations agrees with the values for a vanishing solid volume fraction reported by Soos *et al.* (2008) (shown by the open symbols in figure 11*b*). It is found that the asymptotic mean aggregate mass is proportional to x_L (solid and dashed lines in figure 11*a*, respectively) whose scaling follows from (5.1) using $l_0/\eta \sim (R_\lambda)^{1.16}$ and $R_\lambda \sim \langle\varepsilon\rangle^{0.20}$ (cf. table 2) as $x_L \sim \langle\varepsilon\rangle^{-1.26q} \sim \langle\varepsilon\rangle^{-0.69}$. Further, from figure 11(*b*) it is seen that the asymptotic mean radius of gyration is proportional to $x_L^{1/d_f} \sim \langle\varepsilon\rangle^{-1.26q/d_f} \sim \langle\varepsilon\rangle^{-0.26}$ (solid and dashed line in figure 11*b*). From these findings we conclude that due to turbulent intermittency the asymptotic mean aggregate size exhibits a scaling exponent that is 26% larger than the scaling exponent of the aggregate response function shown by the dotted line in figure 11(*a*). A similar conclusion was drawn by Bałdyga & Podgórska (1998) for droplet breakup.

Let us close this discussion by turning to the experimental data shown in figure 11(*b*) (open symbols) that are described using $q = 0.55$ and $d_f = 2.6$. According to (4.5), this leads to $p = 0.21$ and $n = 4.7$. On the other hand, fitting the experimental data by the Gaussian model (in this case the experimental data shown in figure 11(*b*) is interpreted as the aggregate size at $t = 120$ min, where $c' = 1$ is assumed) gives $C_s' = 1.22 \times 10^7$ (s)$^{-2q}$ and $q = 0.68$ from which $p = 0.26$ and $n = 3.8$. Notably, the former value of p is closer to $p \approx 0.18$ found by Sonntag & Russel (1986) for aggregate breakup in laminar flow whereas the values of n from both models are well within the range of values reported in the literature (Sonntag & Russel 1987*a*).

6. Conclusions

A model for the kinetics of aggregate breakup in a turbulent flow is proposed. It is assumed that the first-order breakup kinetics are governed by the turbulent fluctuations of the local energy dissipation rate that lead to fluctuations in the hydrodynamic stress acting on the aggregates. Under the assumption that breakup is instantaneous when the stress exceeds a certain critical stress (i.e. the local energy dissipation rate exceeds a certain critical value), the (macroscopic) characteristic time of breakup is given by the frequency with which the energy dissipation exceeds a critical value. This critical value depends on the properties of the aggregate. The fluctuations of the local energy dissipation rate are modelled using a multifractal model that provides an accurate description of the PDF of ε. Further, the critical local energy dissipation rate above which breakup occurs is related through a power law to the aggregate mass. The model leads to an expression for $K_B(x)$ that drops to zero below a limiting aggregate mass, x_L.

Two models for the FMD are proposed that differ in the formation of small fragments: a global FMD based on a uniform elementary FMD leads to fragments smaller than x_L while for a global FMD based on a Dirac elementary FMD, the smallest fragments have a mass x_L. Considering a pure breakup process, in both cases the asymptotic CMD becomes proportional to the elementary FMD $\mathscr{G}(\varepsilon, x, y)|_{\varepsilon = \varepsilon_{\max}}$ which is a consequence of the simple expressions used for $\mathscr{G}(\varepsilon, x, y)$, and the result cannot be generalized to an arbitrary elementary FMD. It is further noted that although the asymptotic CMD in the case of a Dirac elementary FMD (that is a monodisperse CMD at x_L) appears infeasible, the time evolution of low-order moments is little influenced by the FMD.

Finally, assuming a Gaussian velocity gradient we derived an expression for $K_B(x)$ that for $x \to 0$ and $x \to \infty$ reduces to an exponential function and a power law. The former is identical to the exponential breakup rate function proposed by Kusters (1991) and Flesch *et al.* (1999). Fitting both the multifractal and the Gaussian model to literature data on the asymptotic aggregate size found in a stirred tank leads to values of the response exponent q that differ by 24%. The value of q (respectively p) from the multifractal model was closer to the value found in laminar flows.

REFERENCES

ADLER, P. M. & MILLS, P. M. 1979 Motion and rupture of a porous sphere in a linear flow field. *J. Rheol.* **23**, 25–37.

BÄBLER, M. U. 2007 Modelling of aggregation and breakage of colloidal aggregates in turbulent flows. PhD Thesis, ETH Zürich.

BÄBLER, M. U. 2008 A collision efficiency model for flow-induced coagulation of fractal aggregates. *AIChE J.* **54**, 1748–1760.

BÄBLER, M. U. & MORBIDELLI, M. 2007 Analysis of the aggregation–fragmentation population balance equation with application to coagulation. *J. Colloid Interface Sci.* **316**, 428–441.

BÄBLER, M. U., SEFCIK, J., MORBIDELLI, M. & BAŁDYGA, J. 2006 Hydrodynamic interactions and orthokinetic collisions of porous aggregates in the Stokes regime. *Phys. Fluids* **18**, 013302.

BAŁDYGA, J. & BOURNE, J. R. 1995 Interpretation of turbulent mixing using fractals and multifractals. *Chem. Engng Sci.* **50**, 381–400.

BAŁDYGA, J. & PODGÓRSKA, W. 1998 Drop break-up in intermittent turbulence: maximum stable and transient sizes of drops. *Can. J. Chem. Engng* **76**, 456–470.

BATCHELOR, G. K. & GREEN, J. T. 1972 The hydrodynamic interaction of two small freely-moving spheres in a linear flow field. *J. Fluid Mech.* **56**, 375–400.

BATCHELOR, G. K. & TOWNSEND, A. A. 1949 The nature of turbulent motion at large wave-numbers. *Proc. R. Soc. Lond.* A **199**, 238–255.

BIFERALE, L., BOFFETTA, G., CELANI, A., LANOTTE, A. & TOSCHI, F. 2005 Particle trapping in three dimensional fully developed turbulence. *Phys. Fluids* **17**, 021701.

BIFERALE, L. & TOSCHI, F. 2005 Joint statistics of acceleration and vorticity in fully developed turbulence. *J. Turbulence* **6**, 40.

BLASER, S. 2000 Break-up of flocs in conctraction and swirling flows. *Colloids Surf.* A **166**, 215–223.

BORGAS, M. S. 1993 The multifractal Lagrangian nature of turbulence. *Phil. Trans. R. Soc. Lond.* A **342**, 379–411.

BRAKALOV, L. B. 1987 A connection between the orthokinetic coagulation capture efficiency of aggregates and their maximum size. *Chem. Engng Sci.* **42**, 2373–2383.

CASTAING, B., GAGNE, Y. & HOPFINGER, E. J. 1990 Velocity probability density functions of high Reynolds number turbulence. *Physica* D **46**, 177–200.

COUFORT, C., BOUYER, D. & LINÉ, A. 2005 Flocculation related to local hydrodynamics in a Taylor-Couette reactor and in a jar. *Chem. Engng Sci.* **60**, 2179–2192.

DELICHATSIOS, M. A. 1975 Model for the breakage rate of spherical drops in isotropic turbulent flows. *Phys. Fluids* **18**, 622–623.

DELICHATSIOS, M. A. & PROBSTEIN, R. F. 1976 The effect of coalescence on the average drop size in liquid–liquid dispersions. *Ind. Engng Chem. Fundam.* **15**, 134–138.

FLESCH, J. C., SPICER, P. T. & PRATSINIS, S. E. 1999 Laminar and turbulent shear-induced flocculation of fractal aggregates. *AIChE J.* **45**, 1114–1124.

FRISCH, U. 1995 *Turbulence*. Cambidge University Press.

FRISCH, U., SULEM, P. L. & NELKIN, M. 1978 A Simple dynamical model of intermittent fully developed turbulence. *J. Fluid Mech.* **87**, 719–736.

GOTOH, T., FUKAYAMA, D. & NAKANO, T. 2002 Velocity field statistics in homogeneous steady turbulence obtained using a high resolution direct numerical simulation. *Phys. Fluids* **14**, 1065–1081.

HARADA, S., TANAKA, R., NOGAMI, H. & SAWADA, M. 2006 Dependence of fragmentation behavior of colloidal aggregates on their fractal structure. *J. Colloid Interface Sci.* **301**, 123–129.

HIGASHITANI, K., IIMURA, K. & SANDA, H. 2001 Simulation of deformation and breakage of large aggregates in flows of viscous fluids. *Chem. Engng Sci.* **56**, 2927–2938.

HINZE, J. O. 1975 *Turbulence, 2nd Edn.* McGraw-Hill.

HORWATT, S. W., FEKE, D. L. & MANAS-ZLOCZOWER, I. 1992*a* The influence of structural heterogeneities on the cohesivity and breakage of agglomerates in simple shear flow. *Powder Tech.* **72**, 113–119.

HORWATT, S. W., MANAS-ZLOCZOWER, I. & FEKE, D. L. 1992*b* Dispersion behavior of heterogeneous agglomerates at supercritcal stress. *Chem. Engng Sci.* **47**, 1849–1855.

JOSEPH, G. G., ZENIT, R., HUNT, M. L. & ROSENWINKEL, A. M. 2001 Particle–wall collisions in a viscous fluid. *J. Fluid Mech.* **433**, 329–346.

KAILASNATH, P., SREENIVASAN, K. R. & STOLOVITZKY, G. 1992 Probability density of velocity increments in turbulent flows. *Phys. Rev. Lett.* **68**, 2766–2769.

KOBAYASHI, M., ADACHI, Y. & OOI, S. 1999 breakage of fractal flocs in a turbulent flow. *Langmuir* **15**, 4351–4356.

KOLMOGOROV, A. N. 1962 A refinement of previous hypotheses concerning the local structure of turbulence in a viscous incompressible fluid at high Reynols number. *J. Fluid Mech.* **13**, 82–85.

KUSTERS, K. A. 1991 The influence of turbulence on aggregation of small particles in agitated vessels. PhD Thesis, Technische Universiteit Eindhoven.

KUSTERS, K. A., WIJERS, J. G. & THOENES, D. 1997 Aggregation kinetics of small particles in agitated vessels. *Chem. Engng Sci.* **52**, 107–121.

LA PORTA, A., VOTH, G. A., CRAWFORD, A. M., ALEXANDER, J. & BODENSCHATZ, E. 2001 Fluid particle accelerations in fully developed turbulence. *Nature* **409**, 1017–1019.

LASHERAS, J. C., EASTWOOD, C., MARTÍNEZ-BAZÁN, C. & MONTAÑÉS, J. L. 2002 A review of statistical models for the break-up of an immiscible fluid immersed into a fully developed turbulent flow. *Intl J. Multiphase Flow* **28**, 247–278.

LATTUADA, M., SANDKÜHLER, P., WU, H., SEFCIK, J. & MORBIDELLI, M. 2003 Aggregation kinetics of polymer colloids in reaction limited regime: experiments and simulations. *Adv. Colloid Interface Sci.* **103**, 33–56.

LIN, M. Y., LINDSAY, H. M., WEITZ, D. A., BALL, R. C., KLEIN, R. & MEAKIN, P. 1989 Universality in colloid aggregation. *Nature* **339**, 360–362.

LUO, H. & SVENDSON, F. 1996 Theoretical model for drop and bubble break-up in turbulent dispersions. *AIChE J.* **42**, 1225–1233.

MENEVEAU, C. & SREENIVASAN, K. R. 1987 Simple multifractal cascade model for fully developed turbulence. *Phys. Rev. Lett.* **59**, 1424–1427.

MENEVEAU, C. & SREENIVASAN, K. R. 1991 The multifractal nature of turbulent energy dissipation. *J. Fluid Mech.* **224**, 429–484.

MOUSSA, A. S., SOOS, M., SEFCIK, J. & MORBIDELLI, M. 2007 Effect of solid volume fraction on aggregation and breakage of colloidal suspensions in batch and continuous stirred tanks. *Langmuir* **23**, 1664–1673.

PANDYA, J. D. & SPIELMAN, L. A. 1982 Floc breakage in agitated suspensions: Theory and data processing strategy. *J. Colloid Interface Sci.* **90**, 517–531.

POPE, S. B. 1990 Langrangian microscales in turbulence. *Phil. Trans. R. Soc. Lond.* A **333**, 309–319.

POPE, S. B. 2000 *Turbulent Flows*. Cambridge University Press.

POTANIN, A. A. 1993 On the computer simulation of the deformation and breakage of colloidal aggregates in shear flow. *J. Colloid Interface Sci.* **157**, 399–410.

PRINCE, M. J. & BLANCH, H. W. 1990 Bubble coalescence and break-up in air-sparged columns. *AIChE J.* **36**, 1485–1499.

RISSO, F. 2000 The mechanisms of deformation and breakage of drops and bubbles. *Multiphase Sci. Tech.* **12**, 1–50.

SAFFMAN, P. G. & TURNER, J. S. 1956 On the collision of drops in turbulent clouds. *J. Fluid Mech.* **1**, 16–30.

SELOMULYA, C., BUSHELL, G., AMAL, R. & WAITE, T. D. 2002 Aggregation mechanisms of latex of different particle sizes in a controlled shear environment. *Langmuir* **18**, 1974–1984.

SHE, Z. S. & LEVEQUE, E. 1994 Universal scaling laws in fully developed turbulence. *Phys. Rev. Lett.* **72**, 336–339.

SONNTAG, R. C. & RUSSEL, W. B. 1986 Structure and breakage of flocs subjected to fluid stresses, I. Shear experiments. *J. Colloid Interface Sci.* **113**, 399–413.

SONNTAG, R. C. & RUSSEL, W. B. 1987a Elastic properties of flocculated networks. *J. Colloid Interface Sci.* **116**, 485–489.

SONNTAG, R. C. & RUSSEL, W. B. 1987b Structure and breakage of flocs subjected to fluid stresses, II. Theory. *J. Colloid Interface Sci.* **115**, 378–389.

SONNTAG, R. C. & RUSSEL, W. B. 1987c Structure and breakage of flocs subjected to fluid stresses, III. Converging Flow. *J. Colloid Interface Sci.* **115**, 390–395.

SOOS, M., MOUSSA, A. S., EHRL, L., SEFCIK, J., WU, H. & MORBIDELLI, M. 2008 Effect of shear rate on aggregate size and morphology investigated under turbulent conditions in stirred tank. *J. Colloid Interface Sci.* **319**, 577–589.

SPICER, P. T. & PRATSINIS, S. E. 1996 Coagulation and fragmentation: Universal steady-state particle size distribution. *AIChE J.* **42**, 1612–1620.

SREENIVASAN, K. R. 1999 Fluid turbulence. *Rev. Mod. Phys.* **71**, S383–S395.

SREENIVASAN, K. R. & ANTONIA, R. A. 1997 The phenomenology of small-scale turbulence. *Annu. Rev. Fluid Mech.* **29**, 435–472.

TENNEKES, H. & LUMLEY, J. L. 1972 *A First Course in Turbulence*. MIT Press.

TOMI, D. T. & BAGSTER, D. F. 1978 The behaviour of aggregates in stirred vessels. Part I: Theoretical considerations on the effects of agitation. *Trans. IChemE* **56**, 1–8.

TSOURIS, C. & TAVLARIDES, L. L. 1994 Breakage and coalescence models for drops in turbulent dispersions. *AIChE. J.* **40**, 395–406.

VEDULA, P. & YEUNG, P. K. 1999 Similarity scaling of acceleration and pressure statistics in numerical simulations of isotropic turbulence. *Phys. Fluids* **11**, 1202–1220.

VEDULA, P., YEUNG, P. K. & FOX, R. O. 2001 Dynamics of scalar dissipation in isotropic turbulence: a numerical and modelling study. *J. Fluid Mech.* **433**, 29–60.

WANG, L.-P., CHEN, S., BRASSEUR, J. G. & WYNGAARD, J. C. 1996 Examination of hypotheses in the Kolmogorov refined turbulence theory through high-resolution simulations. Part 1. Velocity field. *J. Fluid Mech.* **309**, 113–156.

VAN DE WATER, W. & HERWEIJER, J. A. 1999 High order structure functions of turbulence. *J. Fluid Mech.* **387**, 3–37.

WEST, A. H. L., MELROSE, J. R. & BALL, R. C. 1994 Computer simulations of the breakage of colloid aggregates. *Phys. Rev.* E **49**, 4237–4249.

YEUNG, A. K. C. & PELTON, R. 1996 Micromechanics: A new approach to studying the strength and breakage of flocs. *J. Colloid Interface Sci.* **184**, 579–585.

YEUNG, P. K. 2001 Lagrangian characteristics of turbulence and scalar transport in direct numerical simulations. *J. Fluid Mech.* **427**, 241–274.

YEUNG, P. K., POPE, S. B. & KURTH, E. A., LAMORGESE A. G. 2007 Lagrangian conditional statistics, acceleration and local relative motion in numerically simulated isotropic turbulence. *J. Fluid Mech.* **582**, 399–422.

YEUNG, P. K., POPE, S. B., LAMORGESE, A. G. & DONZIS, D. A. 2006a Acceleration and dissipation statistics of numerically simulated isotropic turbulence. *Phys. Fluids* **18**, 065103.

YEUNG, P. K., POPE, S. B. & SAWFORD, B. L. 2006b Reynolds number dependence of Lagrangian statistics in large numerical simulations of isotropic turbulence. *J. Turbulence* **7**, 58.

ZACCONE, A., LATTUADA, M., WU, H. & MORBIDELLI, M. 2007 Theoretical elastic moduli for disordered packings of interconnected spheres. *J. Chem. Phys.* **127**, 174512.